

11 51
10-17-92
P.39

NASA Contractor Report 187141

Experimental Study of Cross Flow Mixing In Cylindrical and Rectangular Ducts

D.S. Liscinsky
*United Technologies Research Center
East Hartford, Connecticut*

A. Vranos
*AB Research Associates
South Windsor, Connecticut*

and

R.P. Lohmann
*Pratt & Whitney Aircraft
East Hartford, Connecticut*

January 1993



(NASA-CR-187141) EXPERIMENTAL
STUDY OF CROSS FLOW MIXING IN
CYLINDRICAL AND RECTANGULAR DUCTS
Final Report (United Technologies
Research Center) 39 p

N93-27680

Unclas

G3/07 0164772

TABLE OF CONTENTS

ABSTRACT	1
1. INTRODUCTION	3
1.1 References	4
2. CROSS-STREAM MIXING in a CYLINDRICAL DUCT	5
2.1 Summary	5
2.2 Nomenclature	5
2.3 Experimental	6
2.3.1 Apparatus	6
2.3.2 Mixing Sections	7
2.3.3 Data Acquisition	9
2.3.4 Data Reduction	11
2.4 Results and Discussion	13
2.4.1 Experiments in a Wasp-Waist Test Section	13
2.4.1.1 Effect of Momentum-Flux Ratio	13
2.4.1.2 Effect of Orifice Shape	17
2.4.2 Experiments in a Straight Test Section	19
2.4.2.1 Effect of Duct Geometry	19
2.4.2.2 Effect of Momentum Flux Ratio	21
2.4.2.3 Effect of Density Ratio	23
2.4.2.4 Effect of Orifice Spacing	25
2.4.2.5 Data Correlation	27
2.5 Conclusions	29
2.6 References	30
3. CROSS-STREAM MIXING in a RECTANGULAR DUCT	31
3.1 Summary	31
3.2 Nomenclature	31
3.3 Experimental	32
3.3.1 Apparatus	32
3.3.2 Data Acquisition	32
3.3.3 Data Reduction/Analysis	33
3.3.4 Mixing Configurations	34
3.4 Results and Discussion	35
3.4.1 Average Concentration Distributions	35
3.4.2 Effect of Flow Conditions	37
3.4.3 Effect of Geometry	37
3.4.3.1 Orifice Spacing	37
3.4.3.2 Orifice Size	38
3.4.3.3 Orifice Shape	39
3.4.3.4 Slot Orientation	41
3.4.4 Time-Resolved Measurements	45
3.4.5 Concentration Probability Density Functions (pdf's)	47
3.4.6 Spatial Covariance	49
3.5 Conclusions	49
3.6 References	50
4. SUMMARY and CONCLUSIONS	51

ABSTRACT

An experimental investigation of non-reacting cross flow jet injection and mixing in cylindrical and rectangular ducts has been conducted with application to a low emissions combustor. Quantitative measurement of injectant concentration distributions perpendicular to the duct axis were obtained by planar digital imaging of the Mie-scattered light from an aerosol seed mixed with the injectant. The flowfield unmixedness was evaluated using (1) a mixing parameter derived from the ratio of the jet concentration fluctuations to the fully mixed concentration, and (2) probability density functions of the concentration distributions. Mixing rate was measured for 45° slanted slot and round orifice injectors.

The cylindrical duct experiments show:

1. Mixing is primarily a function of momentum-flux ratio (J) and injector spacing.
2. Holdeman^{2-3 to 2-8} has shown for round holes in a rectangular duct that jet penetration and mixing is similar when orifice spacing and the square root of J are inversely proportional. This relationship also applied to a 45° slanted slot in a cylindrical duct for a configuration where the adjacent slots did not overlap.
3. When equal area 45° slanted slot and round hole injectors were compared in a configuration which had six equally spaced orifices, better mixing performance was observed for the slanted slots injectors at values $J > 20$. Round holes performed better than the slanted slots at lower values of J for the six injector configuration.
4. Unmixedness of slanted slots is more sensitive to downstream distance than for round holes, which is in agreement with video tapes that show different jet/jet and jet/mainstream interactions for the two types of injectors.

The rectangular duct experiments show:

1. J and orifice geometry significantly affect mixing performance.
2. The inverse proportionality of the square root of J and orifice spacing-to-duct height at the optimum mixing rate applies to slanted slot configurations, although blockage (the web between adjacent orifices) is also an important parameter.
3. For 45° slanted slots, mixing rate is a function of how the orifices are oriented on opposite walls of the duct.
4. Unmixedness values based on time-averaged and time-resolved measurements were found to be nearly equivalent.
5. Probability density functions of the concentration distributions indicate that most of the mixing occurs close to the point of injection.

1. INTRODUCTION

The exhaust gases of gas turbine combustors are a major environmental concern since they contain oxides of nitrogen which may play a significant role in the depletion of ozone¹⁻¹. New engine technology is striving to reduce NO_x emission indices at representative cruise conditions. One promising low NO_x concept is a Rich-Burn / Quick-Mix / Lean-Burn (RQL) combustor¹⁻². In this concept, the primary zone is designed to operate fuel rich. The combustion products then enter the quick-mix region to burnout remaining carbon monoxide and lower the gas temperature. Stoichiometric burning is avoided by operating lean. The key to the concept is rapid and uniform mixing.

This report summarizes the work done under Task Order 2, NASA Contract NAS3-25952. Task 2 was an entitled: "Enhanced Mixing Studies" and was concerned with screening and evaluation of mixing concepts in non-reacting flow for application in the quick-mix zone of an RQL combustor. Quantitative measurement of injectant concentration distributions were obtained by planar digital imaging of the Mie-scattered light from an aerosol seed uniformly mixed with the injectant. A mixing parameter, defined as the ratio of the concentration fluctuation to mean concentration in a plane perpendicular to the main flow direction, was used to evaluate mixer performance.

The application and objectives are most closely related to the cross flow mixing investigations reported by Holdeman et al.^{1-3 to 1-8}. Those studies identified the effects of momentum flux ratio, injector shape, spacing, and location and duct shape on mixing in a rectangular sector geometry with application to gas turbine combustor exit temperature control where 10 to 50% of the total flow enters through the dilution jets. The objective of Task Order 2 was to evaluate mixing techniques in configurations where the mass flow introduced in the quick mixer was up to 70% of the total airflow. Section 2 of the report summarizes the experimental results obtained in a cylindrical duct. Section 3 summarizes the experimental results obtained in a rectangular duct.

1.1 References

- 1-1. Prather, M.J., Wesoky, H.L., Maiké-Lye, R.C., Douglass, A.R., Turco, R.C., Wuebbles, D.J., Ko, M.K.W., and Schmeltekopf, A.L.: The Atmospheric Effects of Stratospheric Aircraft: A First Program Report. NASA Reference Publication 1272, Jan. 1992.
- 1-2. Shaw, R.J.: Engine Technology Challenges for a 21st Century High Speed Civil Transport. AIAA 10th International Symposium on Air Breathing Engines, Sept. 1-6, 1991 (also NASA TM 104363).
- 1-3. Holdeman, J.D., Walker, R.E., and Kors, D.L., "Mixing of Multiple Dilution Jets with a Hot Primary Airstream for Gas Turbine Combustors," AIAA paper 73-1249, Nov. 1973 (see also NASA TM X-71426).
- 1-4. Holdeman, J.D. and Walker, R.E., "Mixing of a Row of Jets with a Confined Crossflow," *AIAA Journal*, Vol. 15, No. 2, Feb. 1977 (see also AIAA paper 76-48 and NASA TM-71821).
- 1-5. Holdeman, J.D., Srinivasan, R., and Berenfeld, A., "Experiments in Dilution Jet Mixing," *AIAA Journal*, Vol. 22, No. 10, Oct. 1984 (see also AIAA Paper 83-1201 and NASA TM-83434).
- 1-6. Holdeman, J.D., Srinivasan, R., Coleman, E.B., Meyers, G.D., and White, C.D., "Effects of Multiple Rows and Non-Circular Orifices on Dilution Jet Mixing," *Journal of Propulsion and Power*, Vol. 3, No. 3, May-June 1987 (see also AIAA paper 85-1104 and NASA TM 86996).
- 1-7. Holdeman, J.D., Srinivasan, R., Reynolds, R., and White, C.D., "Studies of the Effects of Curvature on Dilution Jet Mixing," *Journal of Propulsion and Power*, Vol. 7, No. 4, 1991 (see also, AIAA-87-1953, NASA TM-89878; AIAA-88-3180, NASA TM-100896).
- 1-8. Holdeman, J.D., "Mixing of Multiple Jets with a Confined Subsonic Crossflow; Summary of NASA Supported Experiments and Modeling," AIAA Paper 91-2458, Sacramento, CA., June 1991 (see also NASA TM 104412).

2. CROSS-STREAM MIXING in a CYLINDRICAL DUCT

2.1 Summary

An experimental investigation of mixing in a cylindrical chamber has been studied for transverse injection from slanted slot and round orifice injectors. Momentum-flux ratio, density ratio, and injector geometry were the primary variables. Slanted slots of various size, aspect ratio, and number were studied. Quantitative measurement of injectant concentration distributions were obtained by planar digital imaging of the Mie-scattered light from an aerosol seed uniformly mixed with the injectant. The unmixedness, defined as the ratio of the r.m.s. concentration fluctuation to mean concentration in a plane perpendicular to the main flow direction, was found to be primarily a function of momentum-flux ratio and injector spacing. An optimum spacing is indicated. The data indicate that a density ratio greater than unity retards mixing. It was found that lower values of unmixedness can be obtained with slanted slot injectors than with round hole injectors. However, optimum mixing for slanted slot and round hole injectors does not occur at the same momentum-flux ratio; lower values favor holes, while higher values favor slanted slots. Video tapes of the mixing at very low stream velocity indicate different jet/jet and jet/mainstream interactions for the two types of injectors.

2.2 Nomenclature

A_j	orifice area
C_d	orifice discharge coefficient
\bar{C}	fully mixed mass fraction = $(w_j/w_m)/(1+w_j/w_m) = \theta_{EB}$, Ref. 2-3
F	segregation parameter = $\sqrt{(1-\bar{C})/\bar{C}}$; eq. 2-4
J	jet-to-mainstream momentum-flux ratio = $(\rho_j V_j^2) / (\rho_m V_m^2)$
w_j/w_m	jet-to-mainstream mass flow ratio
R	mixing section radius = 1.25 inches
S	spacing between orifice mid-points, on-center spacing
V_m	mainstream velocity
V_j	jet velocity = $m_j / (\rho_j A_j C_d)$
x/R	normalized downstream location ($x = 0$ at the leading-edge of the orifice)
X	relative unmixedness = $(C_{rms}/C_{avg})/F$

2.3 Experimental

2.3.1 Apparatus

Previous experimental work by Novick²⁻⁹ and numerical study by Smith²⁻¹¹ has indicated that desirable mixing section configurations contract between the rich and lean zones in order to minimize NO_x . Therefore, two different geometries were tested: (1) a wasp-waist configuration, in accordance with previous experience, and (2) a constant area configuration, in order to eliminate duct geometry as a variable. In the wasp-waist configuration, shown in Fig. 2-1, the mainstream contracts through a 30° angle upstream of the mixer, and expands at 21° to a 3 inch duct downstream of the mixer. The straight configuration maintains a 2.5 inch diameter before and after the mixer.

Figure 2-1 is a schematic of the apparatus with the baseline (wasp-waist) mixing section installed. The apparatus consists of three sections: (1) an inlet pipe, (2) a mixing section, and (3) a measuring section with diameters in the ratio of 6:5:7, respectively, as shown in Fig. 2-1. The mainstream flow is conditioned by a series of perforated plates and screens followed by a 7:1 contraction ratio nozzle. The flow velocity is uniform within $\pm 2\%$ at the nozzle exit and was held constant at 10 ft/sec in all cases. Turbulence intensity was not measured. The nozzle is attached to an inlet pipe 6 inches in length and an inside diameter of 3 inches. The inlet pipe attached directly to the mixer. Air to the mixer is plenum fed. The mainstream and jet flows were metered with separate venturi meters supplied by a 400 psi air system. The density of either stream was modified by adding helium through a third venturi well upstream of the test section. The exhaust section downstream of the mixer contains a series of thin (1/16 inch wide) slits which allow optical access at one inch intervals. The first slit is 1.5 inches downstream of the midpoint of the mixing section.

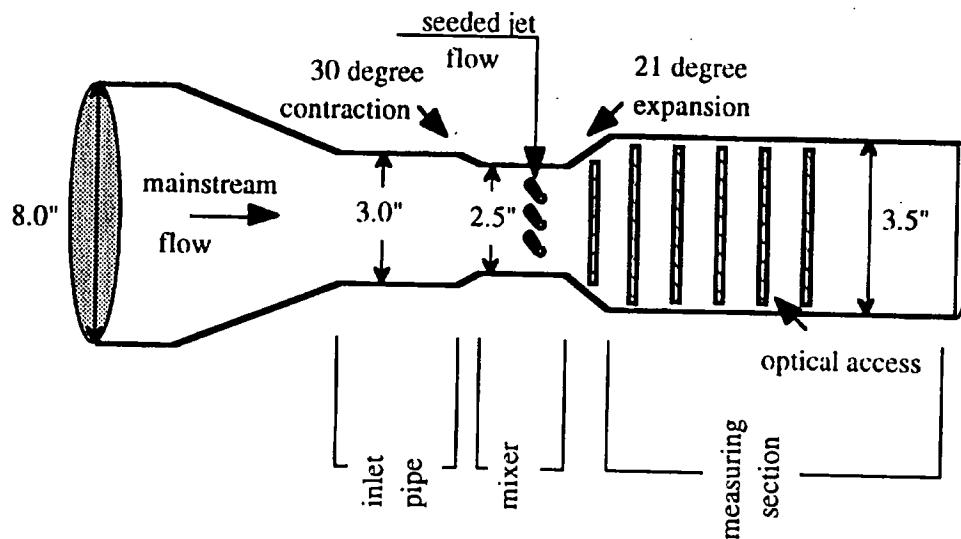


Figure 2-1: RQL Test Apparatus

2.3.2 Mixing Sections

Four interchangeable mixer configurations were studied. The mixers are shown approximately 1/2 scale in Fig. 2-2. Each mixer had 12 equally spaced orifices located along the circumference in the mid-plane of the mixer. The inside diameter and length of each mixer was 2.5 inches. Mixers 2 and 4 have the same physical area. The orifices in mixer 3 have the same width but twice the length as those in mixer 2, thus doubling the area. The orifices in mixer 1 are the same length but twice as wide as those in mixer 2, which again doubles the area. The number of orifices was changed by blocking orifices with tape, so that the symmetric configurations had 2, 3, 4, 6, or 12 orifices. The slots had straight sides with circular ends and were angled 45° to the duct centerline.

		Single Orifice Area (sq in)	Trailing Edge*	Blockage† (12 orifices)
Mixer 1		0.369	0.781	1.49
Mixer 2		0.92	0.387	0.74
Mixer 3		0.190	0.742	1.42
Mixer 4		0.092	0.274	0.52

Figure 2-2: Mixer Configurations

* x projection / R ($R = 1.25$ inches for all tests)

† y projection / S ($S = 0.654$ inches for 12 orifice configurations)

2.3.3 Data Acquisition

Planar digital imaging was used to measure mixing rates. Concentration distributions were measured in a plane normal to the duct axis at several downstream stations for each test configuration. The light scattering technique can be summarized as follows: The jet flow is marked with an oil aerosol (μm size particles). A thin light sheet (0.5 mm thick) is created using a 2W argon-ion laser and a rotating mirror. The flowfield is illuminated by directing the light sheet through one of the imaging ports. A camera, located in the flow downstream of the mixer (end-on view), is programmed to make exposures coincident with the sweep of the beam thru the flow field. The image is then digitized and sent to a computer for storage. The digitized light intensity is proportional to the number of particles in the measurement volume. When one of two streams is marked, the light intensity of the undiluted marked fluid represents mole fraction unity. For a more detailed discussion of the technique see Vranos and Liscinsky²⁻¹³.

Three different cameras were used for planar imaging. All three cameras gave essentially equivalent results, despite differences in operating characteristics. The camera used for the bulk of the data acquisition was a thermoelectrically cooled CCD (CC200, Photometrics, Ltd.). Spatial resolution was $0.01 \times 0.01 \times 0.02$ inch/pixel in a data frame containing 122,500 pixels (350 x 350 format). Each image represents a high resolution time-averaged mole fraction distribution for a 5-10 second exposure. Comparison of results on the basis of mean mole fraction distributions allowed relative evaluation of a large number of flow configurations. Instantaneous concentration distributions were obtained using a low light level vidicon camera. Exposure time was 10 ms. A typical example of the time-resolved data is shown in Fig. 2-3 using a 32-colorscale to represent concentration contours from mole fraction 0.0 to 1.0.

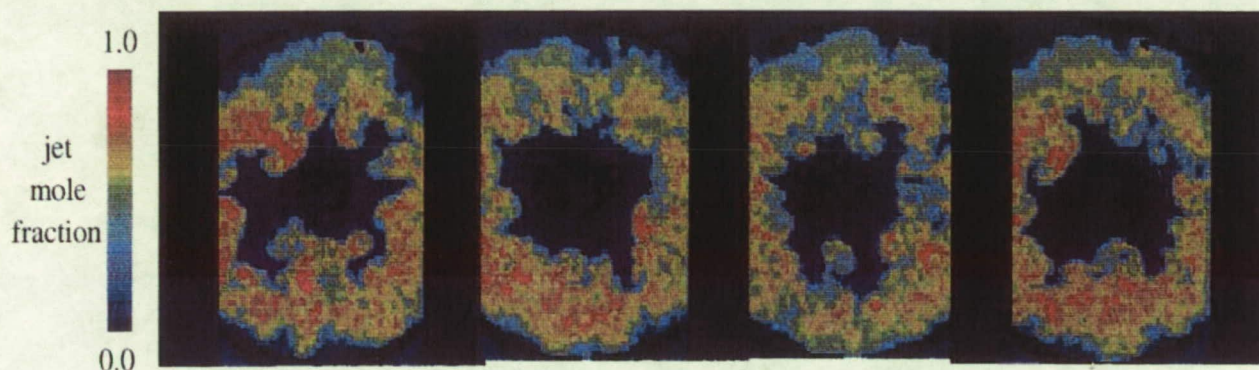


Figure 2-3: Typical Instantaneous Mole Fraction Distributions for 12 slanted slots at $x/R = 1.4$ and $J = 4.6$ (mixer 2)

To obtain absolute mole fraction, the true mole fraction must be known at at least one point in the measurement plane. If undiluted jet fluid is present in the section sampled, then the measured distributions are absolute mole fractions. This is generally not the case, so measured distributions are relative. For some cases the digital image (light signal) was converted to mole fraction by calibration. A trace amount of methane was introduced into the jet flow as a marker. Methane concentration, measured with an on-line hydrocarbon analyzer, provided absolute mole fraction at the sampling location. This measurement allowed conversion of the scattered light intensity measurement to absolute mole fraction (which can then be converted to mass fraction, if desired). For those frames where gas sampling was not available, the calibration was achieved by assuming that the average intensity across the duct was directly proportional to the fully mixed mole fraction.

2.3.4 Data Reduction

The purpose of this investigation was to screen the mixing efficiency of a variety of flow and geometric configurations. Mixing efficiency was measured by a parameter, X , a macroscopic measure of the mixedness or degree of homogeneity of the gas. The mixing parameter X allows comparison of systems with different, or the same, fully mixed concentrations.

Unmixedness is defined as:
$$\frac{C'}{\bar{C}} = \frac{\sqrt{\frac{1}{n} \frac{1}{m} \sum_{j=1}^n \sum_{i=1}^m (C_{ij} - \bar{C})^2}}{\bar{C}} \quad (2-1)$$

where,

n = number of images in data set

m = number of pixels in each image

$$\bar{C} = \frac{1}{n} \frac{1}{m} \sum_{j=1}^n \sum_{i=1}^m C_{ij} = \text{average over all points (all pixels, all realizations)} \quad (2-2)$$

C' = rms fluctuation

Relative unmixedness, X , is defined as: $X = (C' / \bar{C}) / F \quad (2-3)$

where,

$$F = \sqrt{(1 - \bar{C}) / \bar{C}} = (w_j / w_m)^{-1/2} \quad (2-4)$$

$F = 1.57$ for a typical dilution zone jet-to-mainstream flow split of 1:3

$F = 0.57$ for a flow split of 3:1

$F = 0.93$ for the design flow split herein of 1.16:1

\bar{C} = fully mixed mass fraction = fraction of total flow that enters through the jets

In Eq. (2-1), $(C_{ij} - \bar{C})$ is the difference between the instantaneous mass fraction at a particular x, y location in a measuring plane perpendicular to the duct axis and the mean value in that plane, \bar{C} . Summation is with respect to all realizations of the flow at all measuring locations in the plane. The segregation parameter, F , is the maximum value of the rms relative fluctuation for a perfectly segregated system (0,1 bimodal (delta) distribution). Thus, F is the relative fluctuation for the system in the absence of molecular diffusion, and X is the unmixedness relative to this maximum value. Normalization allows comparison of systems of different mean concentrations, \bar{C} , and bounds X at 0 and 1. Thus $X = 0$ corresponds to a perfectly mixed system, and $X = 1$ a perfectly segregated system. It was found that the mean value \bar{C} determined from the combined optical and gas sampling measurements was approximately equal to the the metered value, therefore the metered value was used to compute F .

Because of the large number of pixels per frame, X could be obtained with sufficient accuracy from a single instantaneous exposure. Several exposures were used, nevertheless, to compute X from the time-resolved data. In addition, for this study, it was felt that determination of the mean mass fraction distribution was equally important. Thus, ensemble averaging of the entire field was determined from a 5-10 second time exposure and spatial unmixedness, U_s , was computed as:

$$U_s = \frac{C_{rms}}{C_{avg}} = \frac{\sqrt{\frac{1}{m} \sum_{i=1}^m (\bar{C}_i - C_{avg})^2}}{C_{avg}} \quad (2-5)$$

where,

$$C_{avg} = \frac{1}{m} \sum_{i=1}^m \bar{C}_i \quad (2-6)$$

In Eq. 2-5, C_{ij} is replaced by the ensemble average at a point over all n images, \bar{C}_i . It was found that X , based on the unmixedness of the mean mole fraction distribution (Eq. 2-5 above), correlated well with X as determined from time-resolved measurements (Eq. 2-1). Unmixedness determined from time-resolved and time-averaged data are compared in Table 2-1 which indicates that the unmixedness based on the mean spatial distribution (Eq. 2-5) is less than that of Eq. 2-1, as would be expected. Spatial unmixedness (Eq. 2-5) is thus a useful measure of the total unmixedness, and instantaneous measurements were only acquired for a few test conditions.

I		x/R			
		1.4	2.2	3.0	3.8
5	Eq 1	0.67	0.43	0.45	0.39
	Eq 5	0.52	0.36	0.29	0.21
18	Eq 1	0.42	0.34	0.22	0.20
	Eq 5	0.35	0.25	0.16	0.14
78	Eq 1	0.43	0.37	0.40	0.29
	Eq 5	0.40	0.33	0.22	0.20

Table 2-1: Comparison of Unmixedness for Time-resolved (Eq. 2-1) and Time-averaged (Eq.2- 5) data

2.4 Results and Discussion

Experiments were conducted in two duct configurations, (1) a wasp-waist configuration, in support of ongoing combustion experiments and (2) a straight cylinder, to remove the unknown effects of convergence and divergence.

2.4.1 Experiments in a Wasp-Waist Test Section

2.4.1.1 Effect of Momentum-Flux Ratio

Spatial unmixedness was measured as a function of momentum-flux ratio, J , by varying the slot size while holding the injectant mass flow constant. Slot dimensions are given in Fig. 2-2. A discharge coefficient of 0.6 was assumed in computing V_j from the mass flow average velocity. The mass flow ratio was 1.16. Spatial unmixedness, in duct diameters, is shown as a function of distance in Fig. 2-4 at three momentum flux ratios. The closest allowable measuring plane was at $x/R = 1.2$, a location just downstream of the flange connecting the straight and diverging sections ($x = 0$ at the midpoint of the orifice). The data indicate that substantial mixing has occurred prior to the first measurement station. Since the mass flow ratio was about unity, the spatial unmixedness did not differ significantly from the relative unmixedness X . The data for 12 slot injection suggest the existence of an optimum J , however this may be due to mixer geometry since J and mass flow ratio cannot be studied independently (to hold mass flow and vary J , orifice area, and therefore mixer geometry, must vary).

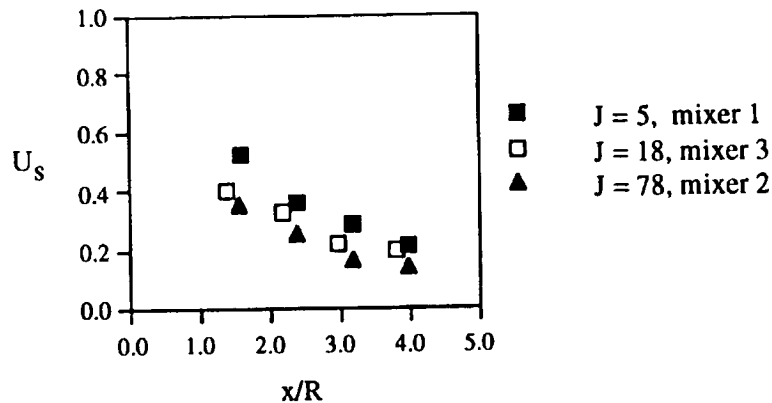


Figure 2-4: Effect of Momentum Flux Ratio on Unmixedness (wasp-waist, 12 slots, $w_j/w_m = 1.16$)

In Fig. 2-5a mole fraction distributions are shown as a function of J for mixer 2 with 6 slot injection at $x/R=1.4$. In this experiment J was varied by changing the mass flow ratio while holding the orifice size constant, therefore the fully mixed mole fraction value increases with increasing J . At $J = 8$ the jets under-penetrate, leaving unmixed mainstream flow in the center of the duct. As J increases, the range of the concentration distribution decreases as mixing improves. An optimum J is not apparent even though it appears that the jets over-penetrate at $J = 95$ (an optimum J was indicated in Fig. 2-4 when J was varied by holding mass flow constant). In Fig. 2-5b mole fraction distributions are shown for mixer 2 as a function of x/R at $J = 8$ and 31 for mixer 2 with 6 slot injection.

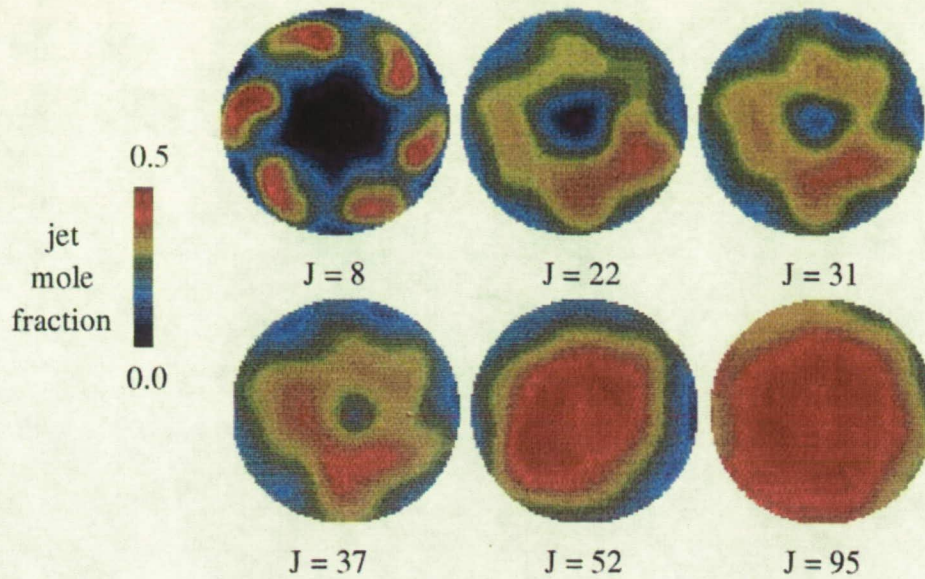


Figure 2-5a: Effect of Momentum-Flux Ratio on Concentration Distribution at $x/R = 1.4$ (6 slot injection, mixer 2)

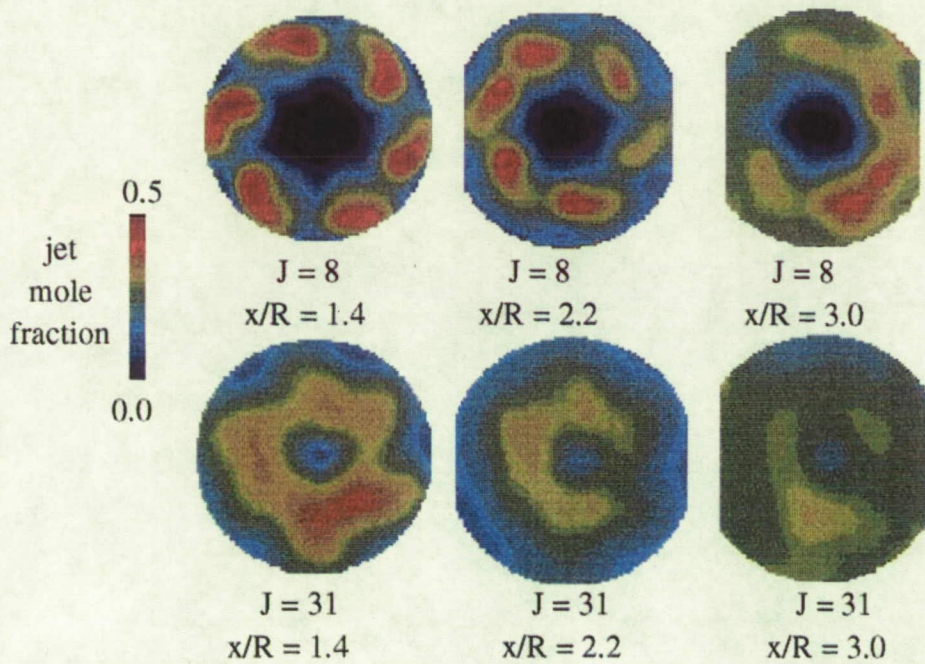


Figure 2-5b: Effect of Momentum-Flux Ratio on Concentration Distribution at $J = 8$ and $J = 31$ (6 slot injection, mixer 2)

2.4.1.2 Effect of Orifice Shape

Spatial unmixedness of round hole and slanted slot injector systems of equal area is compared as a function of J for 6 slot injection in Figs. 2-6a and 2-6b. At $x/R=1.4$ the two systems exhibit roughly the same behavior (Fig. 2-6a), but at $x/R=2.0$ (Fig. 2-6b), it is evident that mixing with the slot injectors has greatly improved while the round injectors only show slight improvement. The difference between round and slanted slot injectors is apparent from these two plots.

- (1) At low J , < 20 , the holes perform better than slots, while at high J they do not. Previous work (1-5) has shown that at equal J , round holes penetrate farther than slanted slots, which is consistent with the better mixing performance shown in Fig. 2-6a. The holes over-penetrate at higher J and appear to be more sensitive to J than the slanted slots.
- (2) In contrast to the holes, the slanted slots continue to mix with downstream distance as shown in Fig. 2-6b. Whatever performance the holes provide occurs immediately after injection, while the slanted slots require more downstream distance to obtain peak performance. Since residence time correlates directly to NO_x formation, the superior mixing performance of slanted slots versus round holes may be outweighed when the application is emission control.

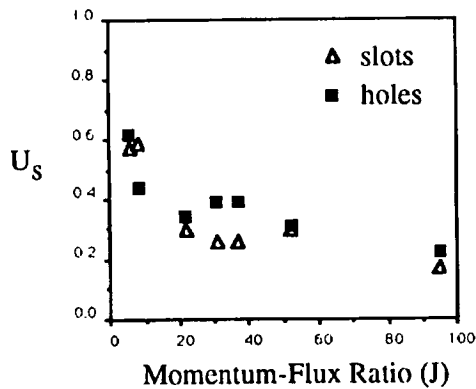


Figure 2-6a: Unmixedness of Equal Area Slanted Slots (mixer 2) and Holes (mixer 4) at $x/R = 1.4$

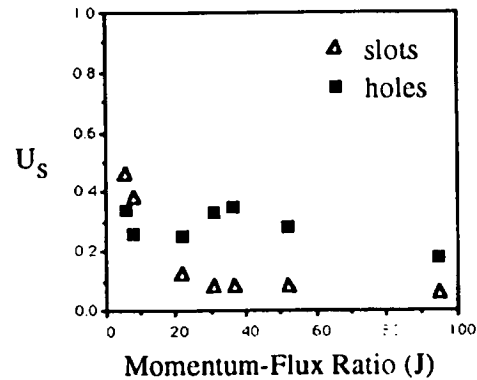


Figure 2-6b: Unmixedness of Equal Area Slanted Slots (mixer 2) and Holes (mixer 4) at $x/R = 2.0$

Representative still frames from movies of low speed flows (Fig. 2-7a-d) further illustrate differences in the jet/jet and jet/mainstream dynamics of slots and round injectors. The jet exiting a round hole forms two counter-rotating vortices of equal strength. The jet penetrates directly toward the center of the duct and the jet cross section becomes more elongated as jet momentum increases. The connecting sheet moves closer to the duct axis, but the vortices tend to remain near the duct wall. The tendency of the vortices to remain near the wall is attributed, in part, to the interaction between neighboring vortices from adjacent jets. Since neighbors rotate in an opposite sense, the induced velocity field is one that tends to translate neighbor pairs toward the duct wall. An additional influence of neighboring jets is to constrain the lateral spreading of the jet and stretch it along its mid-plane; this may contribute to the slightly greater observed penetration of round jets relative to slanted jets. In contrast to the round jet, the slanted jet forms a pair of counter-rotating vortices which are of unequal size and strength. The larger primary vortex forms at the leading edge of the slot and moves towards the duct wall while the smaller vortex moves away from the wall. There is considerable interaction between neighbors early in the injection process. In this case, unlike the round jet system, the induced velocity field is such that the vortex pair rotates about an axis connecting the vortex centers. At the same time, the smaller vortex undergoes a continual stretching deformation as it is drawn in by the upwash of its neighbor pair. It is speculated that this process may play a role in the overall mixing since the stretching process creates surface area while, at the same time, ingesting duct fluid. This would be in accord with the observation that mixing was found to be better with slanted slot injectors than with round injectors given sufficient J and downstream distance.

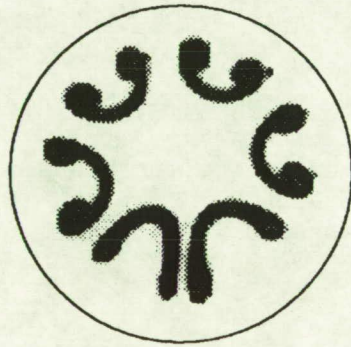


Figure 2-7a: Round Hole at low J

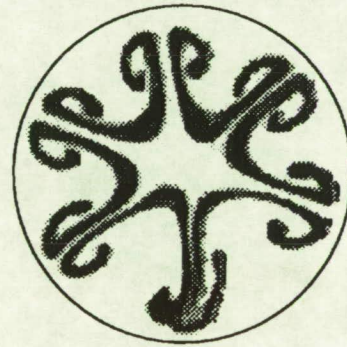


Figure 2-7b: Round Hole at higher J

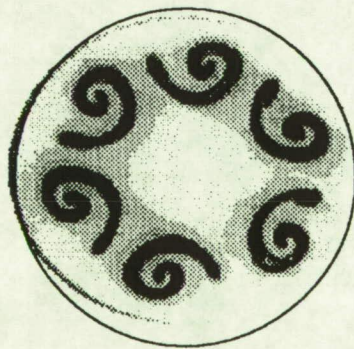


Figure 2-7c: Slanted Slot at low J

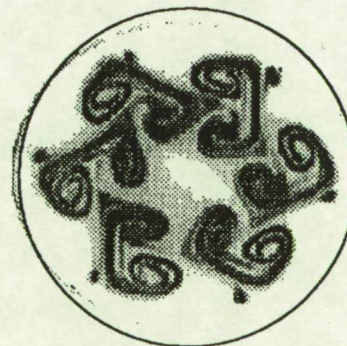


Figure 2-7d: Slanted Slot at higher J

2.4.2 Experiments in a Straight Test Section

2.4.2.1 Effect of Duct Geometry

Spatial unmixedness of the wasp-waist and straight duct configurations are compared as a function of J in Fig. 2-8 at $x/R = 1.4$ with 6 slot injection. In the straight duct configuration, the inlet, mixing section and measurement section, shown previously in Fig. 2-1, all had an inside diameter of 2.5 inches. Except for a slight difference at J values less than 10, the results indicate that mixing performance is not significantly changed by expansion and contraction around the quick-mix zone for the configuration studied.

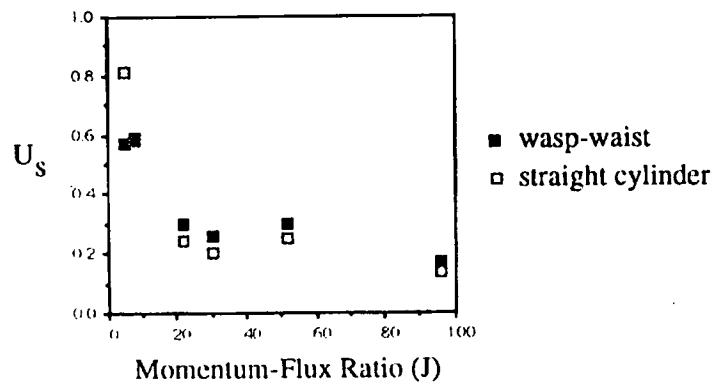


Figure 2-8: Effect of Duct Geometry on Unmixedness for 6 slot injection at $x/R=1.4$ (mixer 2)

2.4.2.2 Effect of Momentum Flux Ratio

The mole fraction distribution for mixer 2 is shown as a function of J and x/R in Fig. 2-9. The momentum-flux ratio was changed by varying the mass flow ratio. At $x/R = 1.4$ and $J = 22$ the jets under-penrate leaving a central core of undiluted mainstream flow. At $J = 52$ the jets over-penrate leaving undiluted mainstream flow at the wall of the duct. In Fig. 2-10, unmixedness is plotted for each of the distributions shown in Fig. 2-9. An optimum J is indicated at $x/R = 1.4$, however farther downstream it appears unmixedness is independent of J .

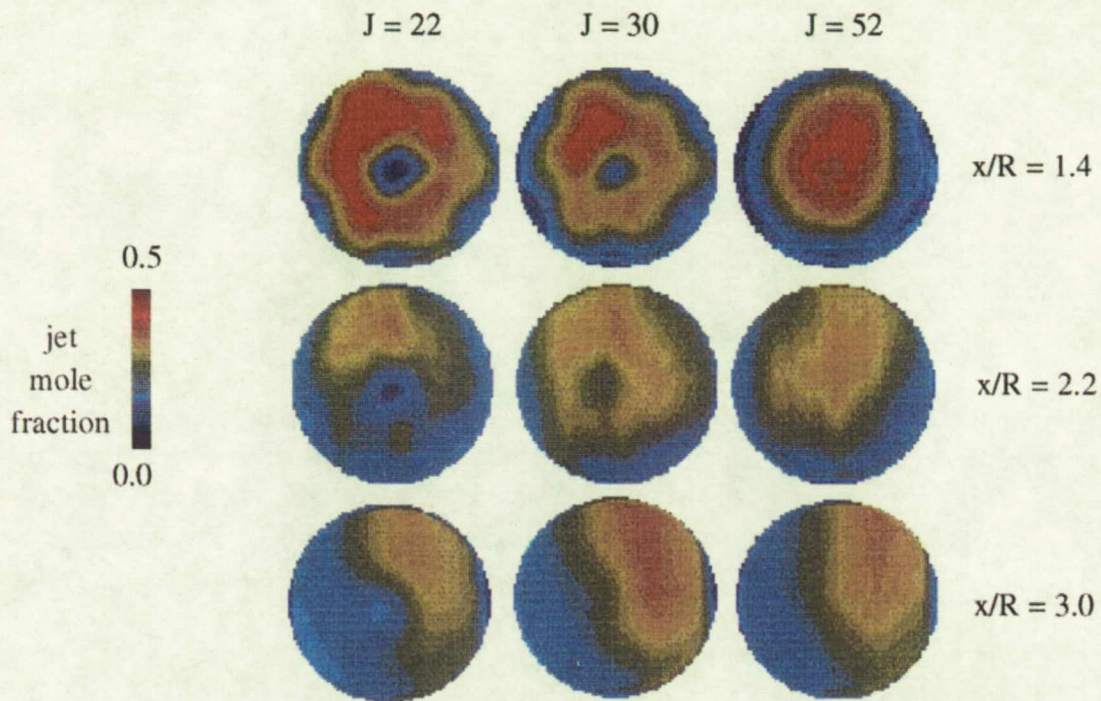


Figure 2-9: Average Concentration Distribution of the Flow through 6 Slanted Slots in a Straight Cylindrical Duct (mixer 2)

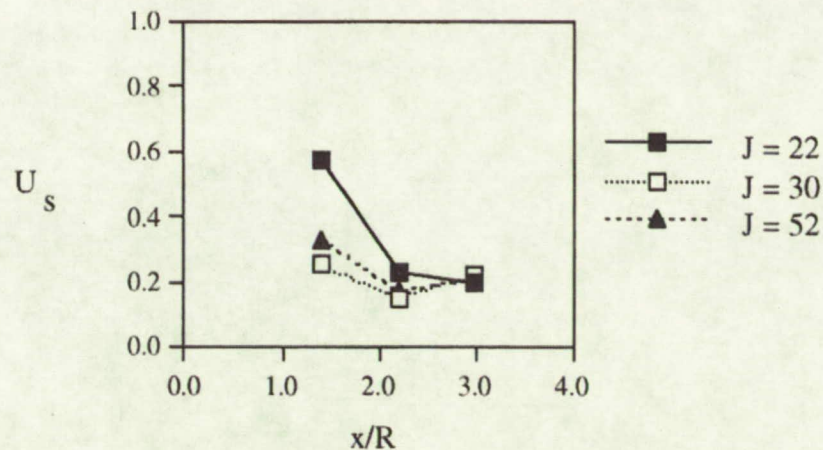


Figure 2-10: Effect of Momentum-Flux Ratio on Unmixedness for 6 Slanted Slots (mixer 2)

2.4.2.3 Effect of Density Ratio

Figs. 2-11a and 2-11b show the dependence of unmixedness on momentum flux ratio for fixed orifice size (mixer 2) and spacing (6 slots) at two density ratios. The figures indicate that mixing is retarded at density ratio above unity. Based on the results of only one test, momentum-flux ratio alone is not sufficient to characterize mixing. Previous studies by Holdeman²⁻³ to 2-8 concluded that density ratio has a secondary effect based on the similarity in profile distributions. In view of those findings the results based on the unmixedness curves warrants further verification.

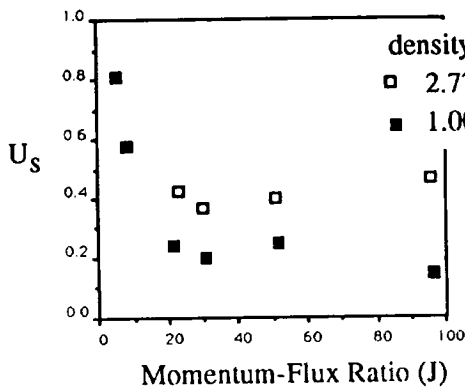


Figure 2-11a: Effect of Momentum-Flux Ratio on Unmixedness at $x/R=1.4$, mixer 2

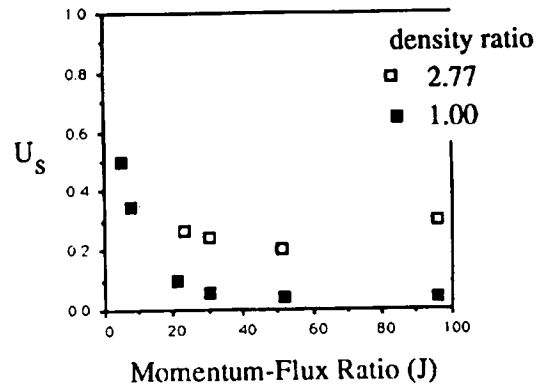


Figure 2-11b: Effect of Momentum-Flux Ratio on Unmixedness at $x/R=2.2$, mixer 2

29

2.4.2.4 Effect of Orifice Spacing

The mole fraction distribution for 3,4,6, and 12 slanted slots at $x/R = 1.4$ for $J = 22$ and $J = 52$ is shown in Fig. 2-12. Jet penetration is affected by the number of orifices, independent of J . This suggests that the overall mixing is determined by the coupling of momentum-flux ratio and orifice spacing. A plot of unmixedness as a function of slot spacing at $J = 52$, shown in Fig. 2-13, indicates that for this J the optimum number of slots is between 6 and 12.

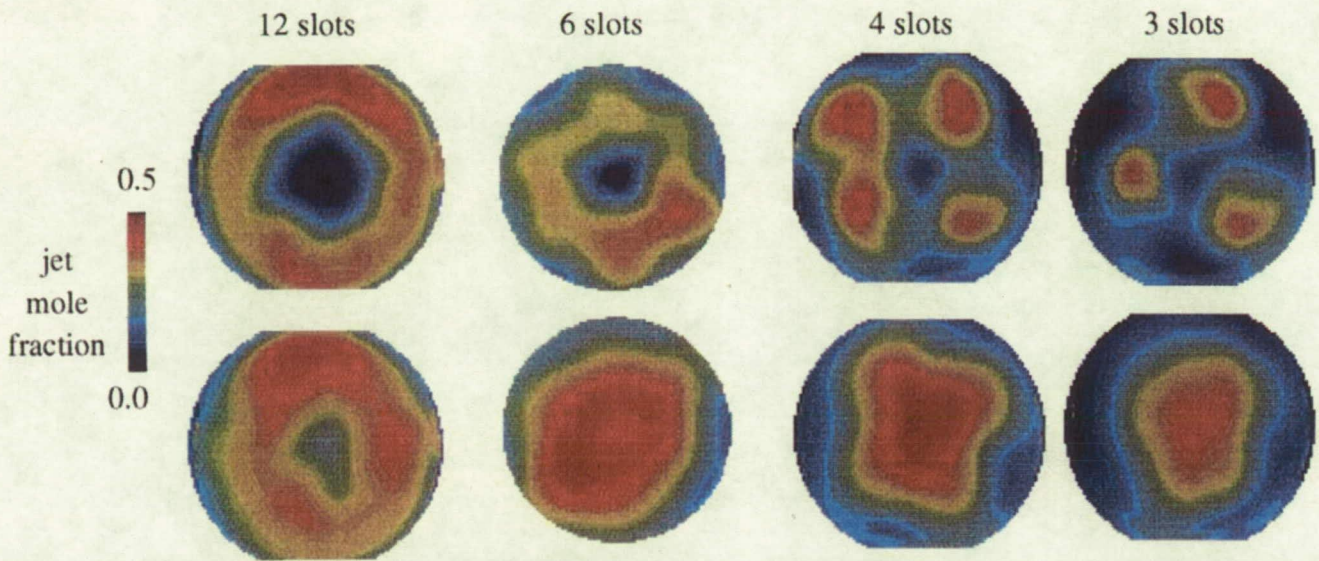


Figure 2-12: Average Concentration Distribution for Four Orifice Spacings at $x/R = 1.4$ for $J = 22$ (top row) and $J = 52$ (bottom row) (mixer 2)

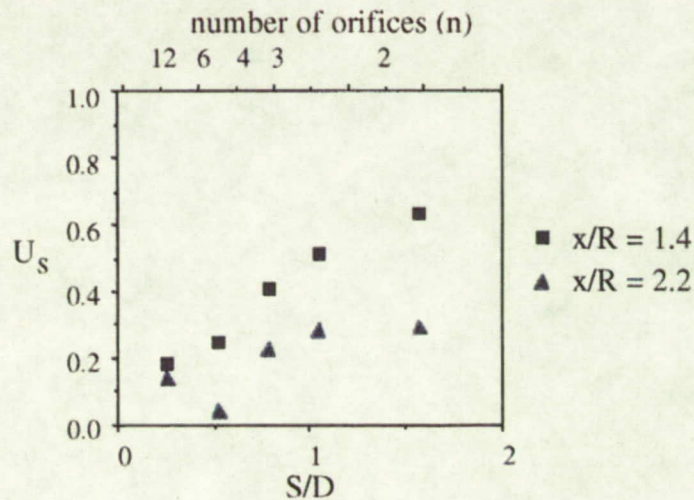


Figure 2-13: Effect of Orifice Spacing on Unmixedness at $J = 52$ (mixer 2)

2.4.2.5 Data Correlation

In an extended series of experiments in rectangular ducts, Holdeman, et al.^{2-3 to 2-8} have shown, on the basis of inspection of mean temperature profiles, that for multi-source injection from equally spaced orifices in rows, jet penetration and mixing can be correlated with a single variable composed of the product of momentum flux ratio and hole spacing, independent of orifice size. The relationship between momentum-flux ratio and hole spacing is given by the expression:

$$C = (S/H)\sqrt{J} \quad (2-7)$$

where,

S = spacing between adjacent orifice centers

H = duct height

J = momentum-flux ratio

optimum mixing was obtained when:

C = 2.5 for single side injection

= 1.25 for 2-sided directly opposed injection (inline)

= 5.0 for 2-sided staggered injection

Eq. 2-7 appeared to give optimum penetration and mixing in a rectangular duct as defined above. To extrapolate this expression to a cylindrical, or can, configuration, corresponding definitions for H, C, and S must be determined. The analog to duct height, H, in a rectangular duct is the duct radius, R, in a cylindrical duct. C = 2.5 is an appropriate choice because this appeared to be the optimum value for one-sided injection in a rectangular duct, which is the limiting case of OD injection into an annular straight duct where the inner radius is 0. There are three choices for S: (1) the outer wall, (2) the half-area radius, or (3) half of the physical radius. The first choice, the outer wall, has been used throughout this report. In hind-sight, it is expected that specifying the optimum S at the outer wall will result in under-penetration, as the width of the can sector converges toward the center. The optimum mixer would require the mean jet trajectory to intersect the point along the duct radius which has equal amounts of mainstream and jet fluid on either side. This corresponds to the half-area radius. Using half the physical radius would render the area/orifice the same in the can as in a rectangular duct, but would not define and optimum jet penetration which would equally divide the can cross section into an equal area circle and annulus. More rigorous extrapolations of Eq. 2-7 to a cylindrical configuration than that presented herein should use an S computed at the half-area radius.

Eq. 2-7 is tested for the present cylindrical configuration in Fig. 2-14 where relative unmixedness is plotted as a function of the variable $Z = (S/H)\sqrt{J}$ with orifice size held constant, mixer 2. The number of slots varied from 2 to 12. It is evident that the data are segregated with respect to the number of slots, and the existence of an optimum Z in the range $5.0 > Z > 2.5$ is indicated. This value is within the range of the optimum constant determined by Holdeman, suggesting that the coupling of J and S/H applies to the cylindrical duct geometry.

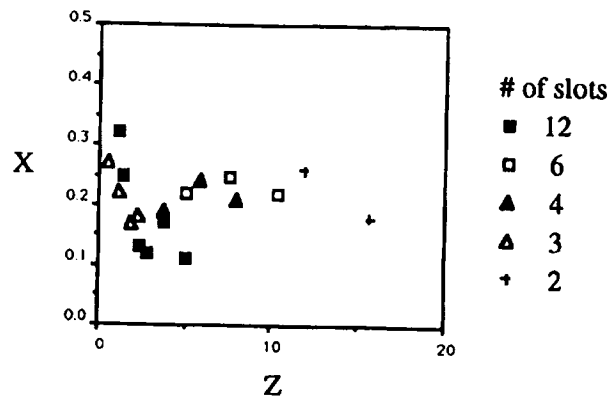


Figure 2-14: Relative Unmixedness (X) as a function of Z at $x/R = 1.4$ (slot size constant, mixer 2)

Between 1987 and 1989 non-reacting cross-flow mixing studies were performed at UTRC in a rectangular apparatus using planar digital imaging to measure concentration distributions transverse to the duct. The test section was 4 inches high and 12 inches wide with provision for injection of fluid through the top and bottom of the chamber. Round orifice injectors were used to study injection from one wall and both walls, in the latter case, opposed holes with staggered centerlines and opposed holes with inline centerlines were tested.

Two configurations were found in the 1987-89 data base which had almost identical conditions to the cylindrical duct experiment. Each rectangular duct configuration consisted of three opposed 0.5 inch diameter holes. One configuration was staggered, while the other was inline. Momentum-flux ratio varied, but S/H remained constant at 0.25 (vs. 0.26 for the 12 slanted slots in the cylindrical duct). Data was collected at $x/H = 1.06$.

A comparison of spatial unmixedness for the two duct configurations as a function of J is presented in Fig. 2-15 as a log-log plot. Agreement between the two duct configurations is good at low momentum-flux ratio. As J increases the data does not agree. It is suspected that the small number of holes (3/side) allowed "end-effects" to influence the rectangular duct data. Since the directly comparable data is limited, any conclusion about the effect of duct geometry would be unwarranted.

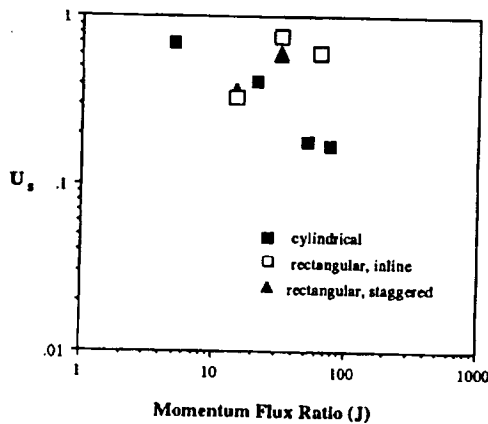


Figure 2-15: Comparison of the Unmixedness in Rectangular and Cylindrical Ducts at $x/H = 1.1$

2.5 Conclusions

- Unmixedness was found to depend on momentum-flux ratio and orifice spacing. The inverse coupling of \sqrt{J} and S/H found previously for rectangular ducts appears to also apply to slanted slots in a cylindrical duct.
- Duct geometry has little effect on unmixedness.
- Mixing rate decreases with increasing density ratio.
- Optimum mixing for slanted slot and round hole injectors does not occur at the same value of J . Lower values favor round holes, while higher values favor slanted slots.
- Lower values of unmixedness can be obtained with slanted slots than with round holes.
- Improved mixing with slanted slot injectors may be due to an initial unsymmetrical vortex pattern characteristic of slanted slots.

2.6 References

- 2-1. Hatch, M.S., Sowa, W.A., Samuelsen, G.S., and Holdeman, J.D., "Jet Mixing into Heated Cross Flow in a Cylindrical Duct: Influence of Geometry and Flow Variations on Mixing of Jets in a Heated Cross Flow," AIAA 92-0773, 30th Aerospace Sciences Meeting, Reno, Jan. 1992 (see also NASA TM 105390)
- 2-2. Hatch, M.S., Sowa, W.A., Samuelsen, G.S., and Holdeman, J.D.: Influence of Geometry and Flow Variation on Jet Mixing and NO Formation in a Model Staged Combustor Mixer. NASA TM 105630, April 1992.
- 2-3. Holdeman, J.D., "Mixing of Multiple Jets with a Confined Subsonic Crossflow; Summary of NASA Supported Experiments and Modeling," AIAA Paper 91-2458, Sacramento, CA., June 1991 (see also NASA TM 104412).
- 2-4. Holdeman, J.D., Srinivasan, R., Reynolds, R., and White, C.D., "Studies of the Effects of Curvature on Dilution Jet Mixing," *Journal of Propulsion and Power*, Vol. 7, No. 4, 1991 (see also, AIAA-87-1953, NASA TM-89878; AIAA-88-3180, NASA TM-100896).
- 2-5. Holdeman, J.D., Walker, R.E., and Kors, D.L., "Mixing of Multiple Dilution Jets with a Hot Primary Airstream for Gas Turbine Combustors," AIAA paper 73-1249, Nov. 1973 (see also NASA TM X-71426).
- 2-6. Holdeman, J.D. and Walker, R.E., "Mixing of a Row of Jets with a Confined Crossflow," *AIAA Journal*, Vol. 15, No. 2, Feb. 1977 (see also AIAA paper 76-48 and NASA TM-71821).
- 2-7. Holdeman, J.D., Srinivasan, R., and Berenfeld, A., "Experiments in Dilution Jet Mixing," *AIAA Journal*, Vol. 22, No. 10, Oct. 1984 (see also AIAA Paper 83-1201 and NASA TM-83434).
- 2-8. Holdeman, J.D., Srinivasan, R., Coleman, E.B., Meyers, G.D., and White, C.D., "Effects of Multiple Rows and Non-Circular Orifices on Dilution Jet Mixing," *Journal of Propulsion and Power*, Vol. 3, No. 3, May-June 1987 (see also AIAA paper 85-1104 and NASA TM 86996).
- 2-9. Novick, A.S., and Troth, D.L., "Low NO_x Heavy Fuel Combustor Concept," NASA CR-16537, 1981
- 2-10. Smith, C.E., Talpallikar, M.V., and Lai, M.C., "Rapid Mix Concepts for Low Emission Combustors in Gas Turbine Engines," NASA CR-185292, Oct. 1990, pp. 2.
- 2-11. Smith, C.E., Talpallikar, M.V., and Holdeman, J.D., "A CFD Study of Jet Mixing in Reduced Flow Areas for Lower Combustor Emissions," AIAA Paper 91-2460, Sacramento, CA., June 1991 (see also NASA TM 104411).
- 2-12. Talpallikar, M.V., Smith, C.E., Lai, M.C., and Holdeman, J.D., "CFD Analysis of Jet Mixing in Low NO_x Flametube Combustors," ASME Paper 91-GT-217, Orlando, FL., June 1991 (see also NASA TM 104466).
- 2-13. Vranos, A. and Liscinsky, D.S., "Planar Imaging of Jet Mixing in Crossflow," *AIAA Journal*, 26, 11, Nov. 1988, pp 1297-98.

3. CROSS-STREAM MIXING in a RECTANGULAR DUCT

3.1 Summary

An experimental investigation of non-reacting cross-stream jet injection and mixing in a rectangular duct has been conducted with application to a low emissions combustor. Planar digital imaging was used to measure concentration distributions in planes perpendicular to the duct axis. Mixing rate was measured for 45° slanted slot and round orifice injectors. It is shown that (1) mixing improves continuously with increasing momentum-flux ratio, (2) given a momentum-flux ratio, there is an optimum orifice spacing, (3) mixing is more dependent on injector geometry than mass flow ratio, (4) mixing is influenced by relative slot orientation, and (5) jet structure is different for round holes and slanted slots injectors. The utility of acquiring multipoint fluctuating properties of the flow field is also demonstrated.

3.2 Nomenclature

C_{avg}	fully mixed mass fraction = $(w_j/w_m)/(1+w_j/w_m) = \theta_{EB}$, Ref. 3-1
H	duct height at injection plane = 4 in
J	jet-to-mainstream momentum-flux ratio = $(\rho_j V_j^2) / (\rho_m V_m^2)$
L	length of the orifice, longest dimension (see Table 1)
S	spacing between orifice mid-points, on-center spacing
U_s	spatial unmixedness parameter (Eq. 1)
V_m	mainstream velocity = 10 ft/s
V_j	jet velocity = $m_j / (\rho_j A_j C_d)$
W	width of the orifice, shortest dimension (see Table 1)
w_j/w_m	jet-to-mainstream mass flow ratio
x	downstream location, $x = 0$ at the upstream edge of the orifice

3.3 Experimental

3.3.1 Apparatus

Figure 3-1 is a schematic representation of the apparatus. The apparatus consists of 3 parallel contiguous ducts of rectangular cross section, simulating a sector of an annular combustor. Sector width is 12 inches. The inner duct height is 4 inches. The outer ducts (shrouds), which supply the injectant gas, are 1 inch in height. These are separated from the inner duct by removable, 0.12 inch thick flat plates. The injectant is fed from the shrouds to the inner duct through orifices of various sizes and shapes that are machined into the plates. Mass flow to each of the 3 ducts is controlled independently using venturi flowmeters. The maximum variation in the mean approach velocity of the mainstream flow was 6% with a turbulence level of 1.3%.

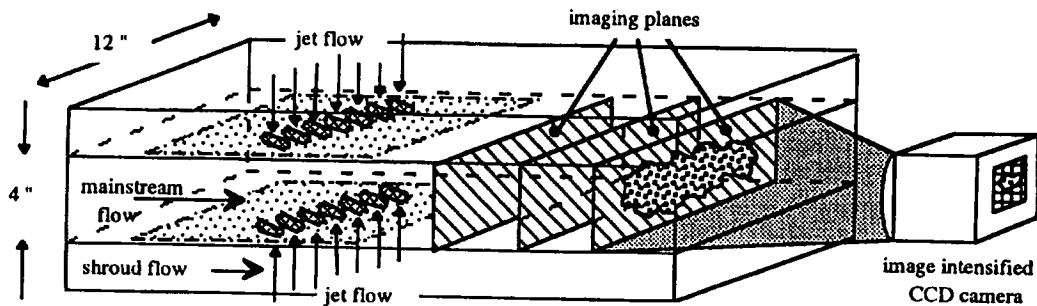


Figure 3-1: Experimental Configuration used to Measure Planar Concentration Distributions

3.3.2 Data Acquisition

Planar digital imaging was used to measure optically concentration distributions in planes perpendicular to the duct axis 1, 2, 3, and 4 inches downstream of the midpoint of the orifice for each test configuration and flow condition. The Mie-scattering technique can be summarized briefly. The jet flow is marked with an oil aerosol (mm sized particles). A light sheet (0.02 inch thick) is created using a 2W argon-ion laser and a rotating mirror. The flow field is illuminated by passing the light sheet through a window in the side wall of the test section. A solid state camera, located inside the duct 2.5 ft downstream of the orifice centerline, is focused on the illuminated plane (end-on view). The camera is programmed to make exposures coincident with the sweep of the beam through the flow field. The image is digitized and sent to a computer for storage. The scattered light intensity is proportional to the number of particles in the measurement volume. If only one of two streams is marked, the light intensity of the undiluted marked fluid represents mole fraction unity. For a more detailed discussion of the technique see Vranos and Liscinsky³⁻⁷.

An image intensified, thermo-electrically cooled, CCD camera was used to record the images. Time-averaged (5 second exposure) measurements of the concentration distribution were obtained for all tests. Time-resolved (50ms exposure) measurements were obtained for two configurations: opposed rows of inline slanted slots (code SSE in Table 3-1) and opposed rows of staggered slanted slots (code SSG in Table 3-1). All images recorded the entire duct cross section at a spatial resolution of 0.02 x 0.02 x 0.02 inches in a data frame containing 110,592 pixels (576 x 192 format).

3.3.3 Data Reduction/Analysis

The mole fraction at at least one point in the flow field must be known in order to compute absolute mole fraction distribution from the digital image. This can be done using a hydrocarbon tracer and a sampling probe³⁻⁸, but, for these experiments, a simple approximation was made. The fully mixed mole fraction, C_{avg} , is calculated from the metered mass flows. Since the scattered light intensity distribution across the entire duct is known for each frame, the average light intensity in each image is proportional to C_{avg} . Each pixel in the image was subsequently normalized to obtain a local average mole fraction. It is shown in Ref. 3-8 that this is an acceptable approximation.

Mean concentration distributions, i.e. spatial distributions of the local mean concentration, can be used to define the mixing effectiveness of each configuration. In a previous paper³⁻⁸, an unmixedness parameter was defined to allow rapid screening of a variety of flow and geometric configurations in a cylindrical duct. The same spatial unmixedness parameter, U_s , defined by Eq. 3-1, was used in this investigation. In a perfectly mixed system $U_s = 0$.

$$U_s = \frac{C_{rms}}{C_{avg}} = \frac{\sqrt{\frac{1}{m} \sum_{i=1}^m (\bar{C}_i - C_{avg})^2}}{C_{avg}} \quad (3-1)$$

where,

n = number of pixels in each image

\bar{C}_i = average concentration at a pixel

$C_{avg} = \frac{1}{m} \sum_{i=1}^m \bar{C}_i$ = average concentration over all pixels in an image

3.3.4 Mixing Configurations

Table 3-1 identifies the 7 orifice plate configurations tested. The configuration sketches are drawn approximately 1/2 scale in Table 3-1. Two injector shapes were studied: (1) slanted slots, aspect ratio 4:1, and (2) round holes. The slots had circular ends and were slanted 45° to the mainstream flow direction. Injection was 2-sided. Discharge coefficients were measured for each orifice shape and used to set 4 momentum-flux ratios (J): 16, 36, 64, 100. The mainstream flow was held constant at 10 ft/sec for all tests.







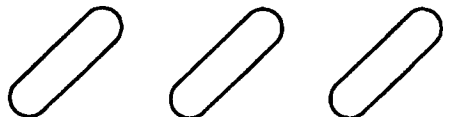
CODE	CONFIGURATION	ASPECT RATIO	H/W	TRAILING*		
				S/H	EDGE BLOCKAGE†	
RHD		1:1	8.0	0.50	0.125	0.250
SSB		4:1	17.5	0.25	0.178	0.711
SSE		4:1	17.5	0.50	0.178	0.355
SSF		4:1	17.5	0.50	0.178	0.355
SSG		4:1	17.5	0.50	0.178	0.355
SSH		4:1	17.5	0.50	0.178	0.355
SSE4		4:1	8.8	0.50	0.355	0.711

Table 3-1: Orifice Plate Configurations
(dotted lines represent orifices on the opposite wall)

* x projection / H (H = 4 inches for all tests)

† y projection / S

3.4 Results and Discussion

3.4.1 Average Concentration Distributions

Distributions of average mole fraction are shown as a function of downstream distance at momentum-flux ratios of 16 and 36 in Fig. 3-2. The orifice configuration consists of opposed rows of inline slanted slots (code SSE in Table 3-1). The top and bottom slots slant in the same direction (parallel). The individual jets are still discernible at the first downstream location. In contrast to a round orifice jet (Fig. 3-7), the slanted slot jet forms a pair of counter-rotating vortices which are of unequal size and strength. The vortex formed at the upstream edge of the slot is larger and penetrates farther than the vortex formed at the downstream edge. The vortex pair is rotated so that the bulk of jet fluid is found toward the side of the slot that is upstream, thereby identifying the direction in which the slot is slanted (In Fig. 3-2 the upstream edge of the slot is on the right). In addition, the main body of the jet is displaced relative to the midpoint of the slot.

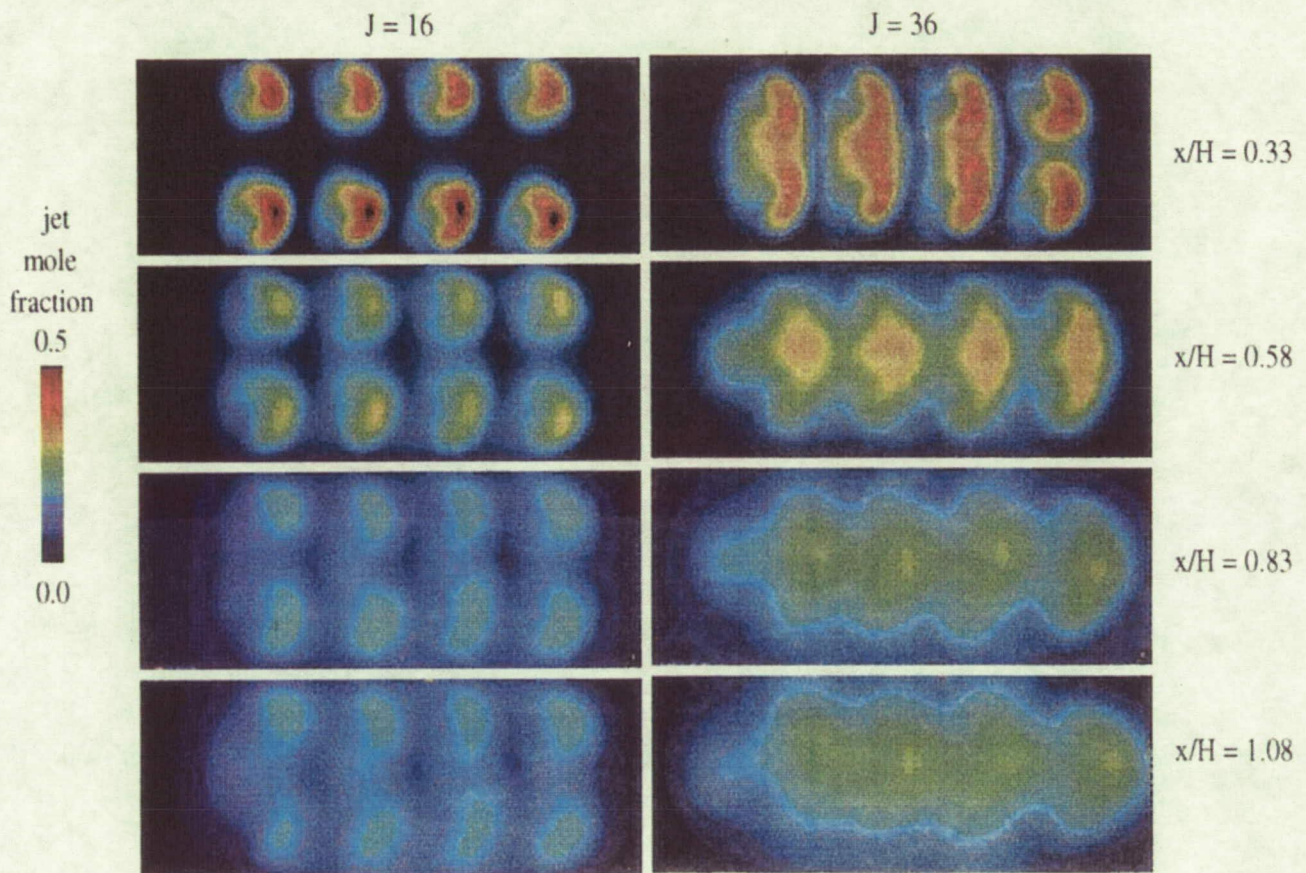


Figure 3-2: Average Concentration Distributions of the Flow through Opposed Inline 45° Slanted Slots, code SSE in Table 3-1

3.4.2 Effect of Flow Conditions

The effect of momentum-flux ratio on unmixedness is shown in Fig. 3-3 for a row of opposed inline slanted slots (code SSE in Table 3-1). Mixing rate was found to increase continuously with increasing J . None of the test configurations showed an optimum value of J over the range studied.

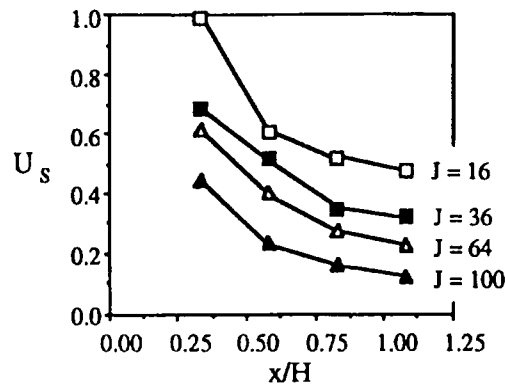


Figure 3-3: Effect of Momentum-flux ratio on Opposed Inline Slanted Slots, $S/H = 0.5$, code SSE in Table 3-1

A value of U_s below 0.1 was not observed in any configuration. In most configurations there was a noticeable decrease in mixing rate beyond $x/H = 0.5$. In some cases the change in U_s from $x/H = 0.8$ to $x/H = 1.0$ was not significant. Therefore, the initial mixing rate is vital in emissions control.

3.4.3 Effect of Geometry

3.4.3.1 Orifice Spacing

U_s is shown as a function of orifice spacing at $J = 36$ for opposed rows of inline slanted slots in Fig. 3-4. Mixing improved at closer spacing. Previously, Holdeman³⁻², has shown, on the basis of mean temperature distributions, that for multi-source injection from equally spaced round orifices in rows, mixing can be correlated by a single variable composed of the product of momentum-flux ratio and orifice spacing, independent of orifice size. Optimum penetration and mixing for any given configuration is obtained when the square root of the momentum-flux ratio and orifice spacing are inversely proportional so that:

$$C = (S/H) \sqrt{J} \quad (3-2)$$

where,

- S = spacing between adjacent orifice mid-points
- H = duct height
- J = momentum-flux ratio
- C = 2.5 for single side injection
- = 1.25 for 2-sided opposed inline injection
- = 5.0 for 2-sided opposed staggered injection

From Eq. 2, at $J = 36$, the optimum $S/H = 0.21$. The trend of the data in Fig. 3-5 supports the value calculated using Eq. 2, in that mixing was better at $S/H = 0.25$. The inline slots at $S/H = 0.5$ are more widely spaced than the optimum, and mixing is slower as shown in Fig. 3-4 and confirmed by the distributions shown for $J = 36$ in Fig. 3-2. Holdeman^{3,2} has attributed this phenomenon to over-penetration at wide spacing.

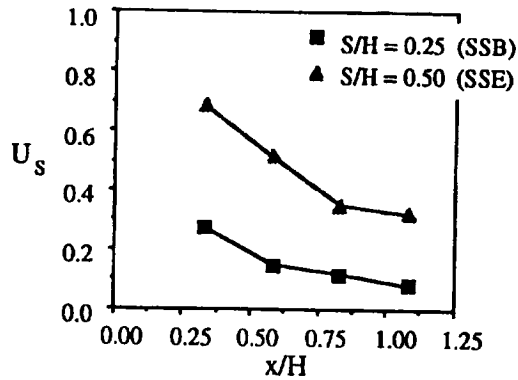


Figure 3-4: Effect of Orifice Spacing on Unmixedness for Opposed Inline Slanted Slots, $J = 36$ (codes are from Table 3-1)

3.4.3.2 Orifice Size

The effect of orifice size is shown in Fig. 3-5 for opposed inline slanted slots (code SSE and SSE4 in Table 3-1). The slot area was enlarged by a factor of 4 while maintaining the same aspect ratio (4:1), orifice spacing (S/H) and momentum-flux ratio. Mixing improved as orifice size increased. However, when the smaller orifices (code SSB in Table 3-1) were tested with the same blockage (defined in Table 3-1) and J , i.e. a geometrically similar injector configuration, U_s is the same. Therefore, it may be that the improvement evident in Fig. 3-5 is due to a smaller blockage between adjacent slots rather than a change in orifice size. In other words, it appears that injector geometry and distribution are controlling the mixing rate rather than mass flow ratio. The results indicate that blockage is an important factor for non-symmetrical orifices, in addition to the parameter S/H .

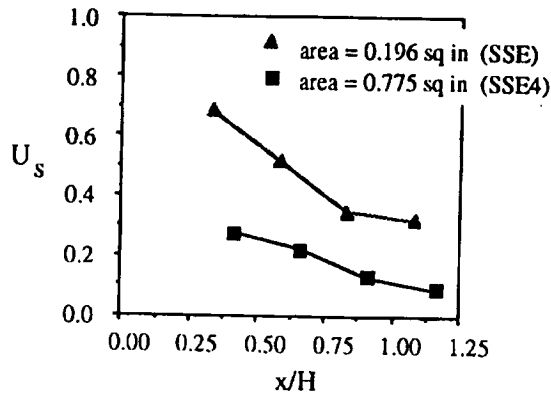


Figure 3-5: Effect of Orifice Size on Unmixedness for Opposed Inline Slanted Slots, $J = 36$ (codes are from Table 3-1)

3.4.3.3 Orifice Shape

The effect of orifice shape is shown in Fig. 3-6. Unmixedness is shown for inline slanted slots (code SSE in Table 3-1) and round holes (code RHD in Table 3-1) at $J = 16, 36,$ and 100 . The orifice spacing (S/H) and mass flow ratios are equal, however the blockage of the round holes is 20% less. U_s was found to be about the same for both configurations. Given the different initial vortex structure of the jet fluid (illustrated in Figs. 3-2 and 3-7) different mixing rates might have been expected for the two orifice shapes. However, vortex development may only effect mixing when the orifices are more closely spaced so that interaction of the adjacent jets is stronger. This would be the case at the optimum spacing, $S/H = 0.21$ for $J = 36$.

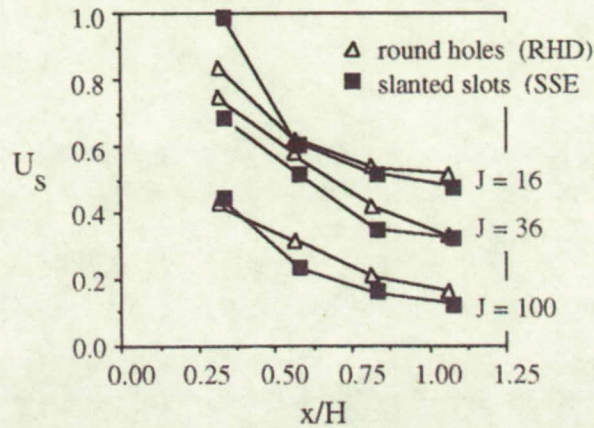


Figure 3-6: Effect of Orifice Shape on Unmixedness for Opposed Inline Orifices, $S/H = 0.5$ (codes are from Table 3-1)

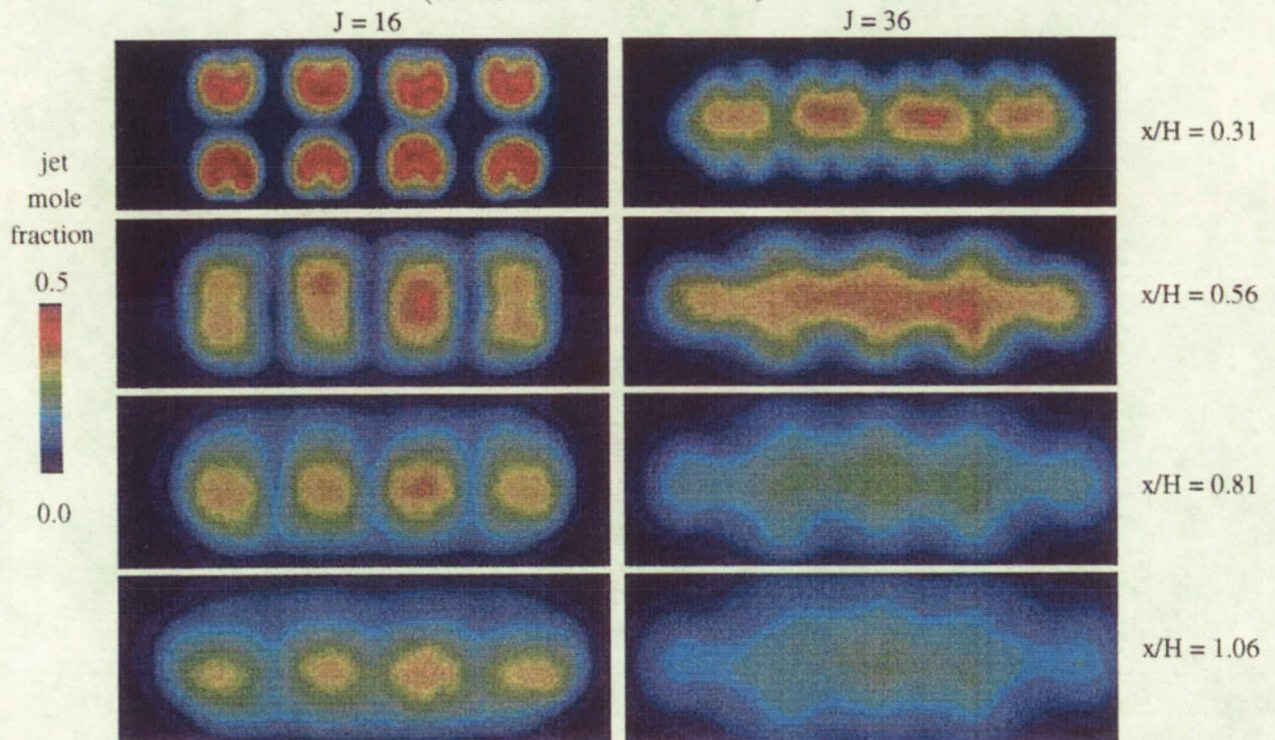


Figure 3-7: Concentration Distributions of the Flow through Opposed Inline Round Holes, code RHD in Table 3-1

3.4.3.4 Slot Orientation

Mixing rate can be modified by changing the relative slot orientation, that is by slanting the slots on the top and bottom duct walls in opposite directions relative to each other ("crossed") so that the relative angle between top and bottom slots is 90° . The effect of the "crossed" configuration is shown in Fig. 3-8 for $J=36$ and $S/H=0.5$. When the slots are inline and "crossed" as in code SSF in Table 3-1, U_s was the same as if the slots were inline and "parallel" as in code SSE in Table 3-1. However, when the slots are staggered and "crossed" as in code SSH in Table 3-1, U_s was significantly higher than if the staggered slots were "parallel" as in code SSG in Table 3-1.

As discussed previously, and as shown in Fig. 3-9a (code SSE), the main body of the jet from a slanted slot is displaced relative to the midpoint of the orifice. Therefore, in a staggered configuration "crossing" the slots will tend to re-align the jets with the orifice, rather than displace the jets as shown in Fig. 3-9a by codes SSG and SSH. As predicted by Eq. 2, $S/H=0.5$ is not optimum for an inline configuration, but closer to the optimum $S/H=0.8$ for a staggered configuration. By "crossing" the slots the advantage of the staggered configuration at this S/H was lost, as shown by comparing the data from codes SSG and SSH in Fig. 3-9b.

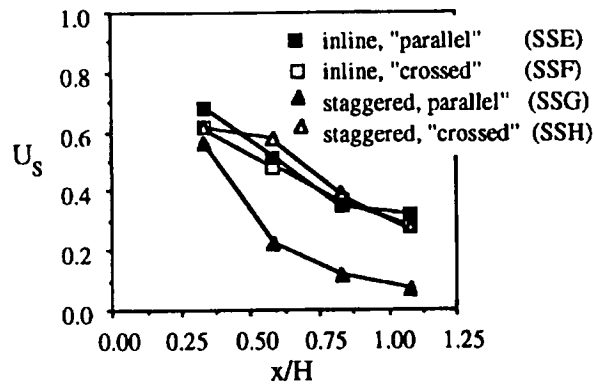


Figure 3-8: Effect of Slot Orientation on Unmixedness for opposed slanted slots, $J = 36$, $S/H = 0.5$ (codes are from Table 3-1)

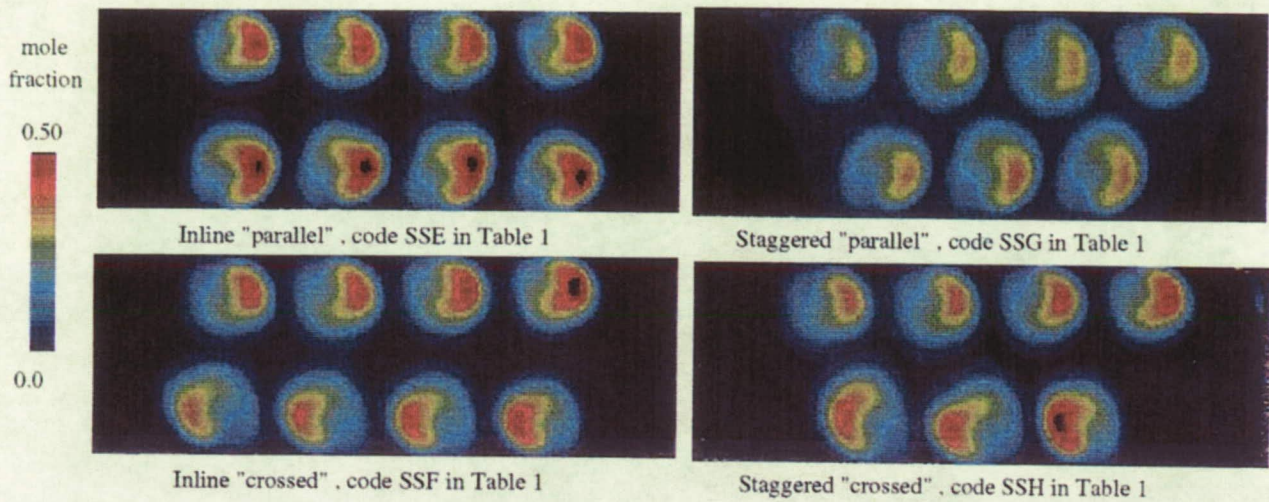


Figure 3-9a: Concentration Distributions of Opposed Slanted Slots
at $J = 16$, $S/H = 0.5$, $x/H = 0.33$

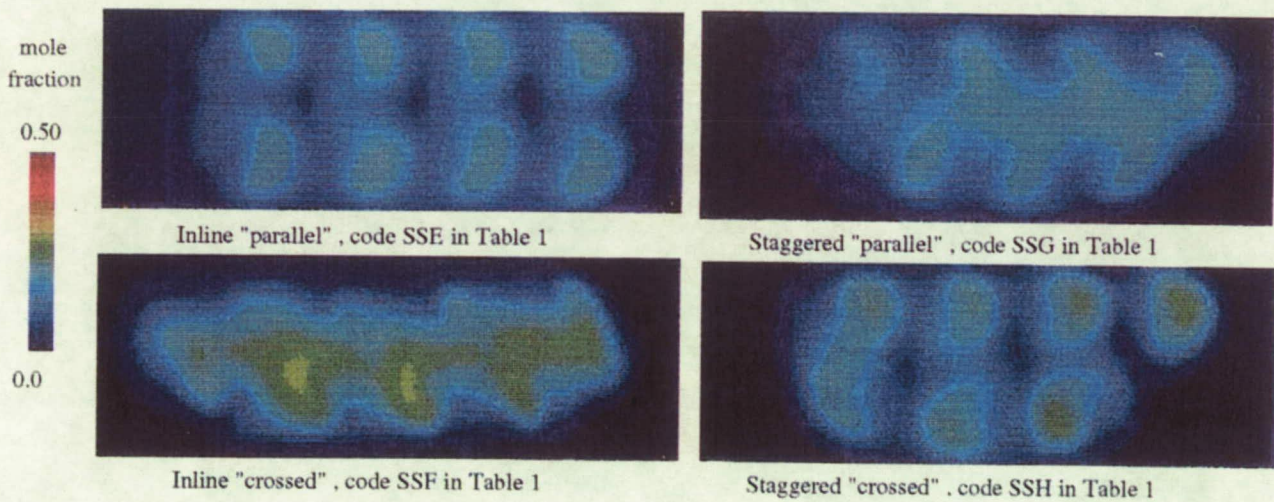


Figure 3-9b: Concentration Distributions of Opposed Slanted Slots
at $J = 16$, $S/H = 0.5$, $x/H = 0.83$

3.4.4 Time-Resolved Measurements

U_s is a useful performance measure which allows rough screening of various injector configurations. To further assess performance, time-resolved data can be used in conjunction with a chemical model to estimate weighted, mean pollutant formation rates. Absent a chemical calculation, the statistical properties of the flowfield might be useful for differentiating those configurations with low, but comparable, values of U_s . Time-resolved measurements were made for opposed inline (code SSE in Table 3-1) and opposed staggered (code SSG in Table 3-1) slanted slots at $J = 36$ and $x/H = 0.33$. For both configurations the data set is comprised of 300 images. Mean concentration distribution, a typical instantaneous concentration distribution, the rms concentration fluctuation distribution, and the relative concentration fluctuation distribution are shown in Fig. 3-10. Based on the average concentration distribution only, the staggered configuration was shown to have the lower value of U_s . A comparison of the rms concentration distribution leads to the same conclusion. Highest fluctuations are located between adjacent slots, indicating that the spacing is too large, consistent with Eq. 3-2.

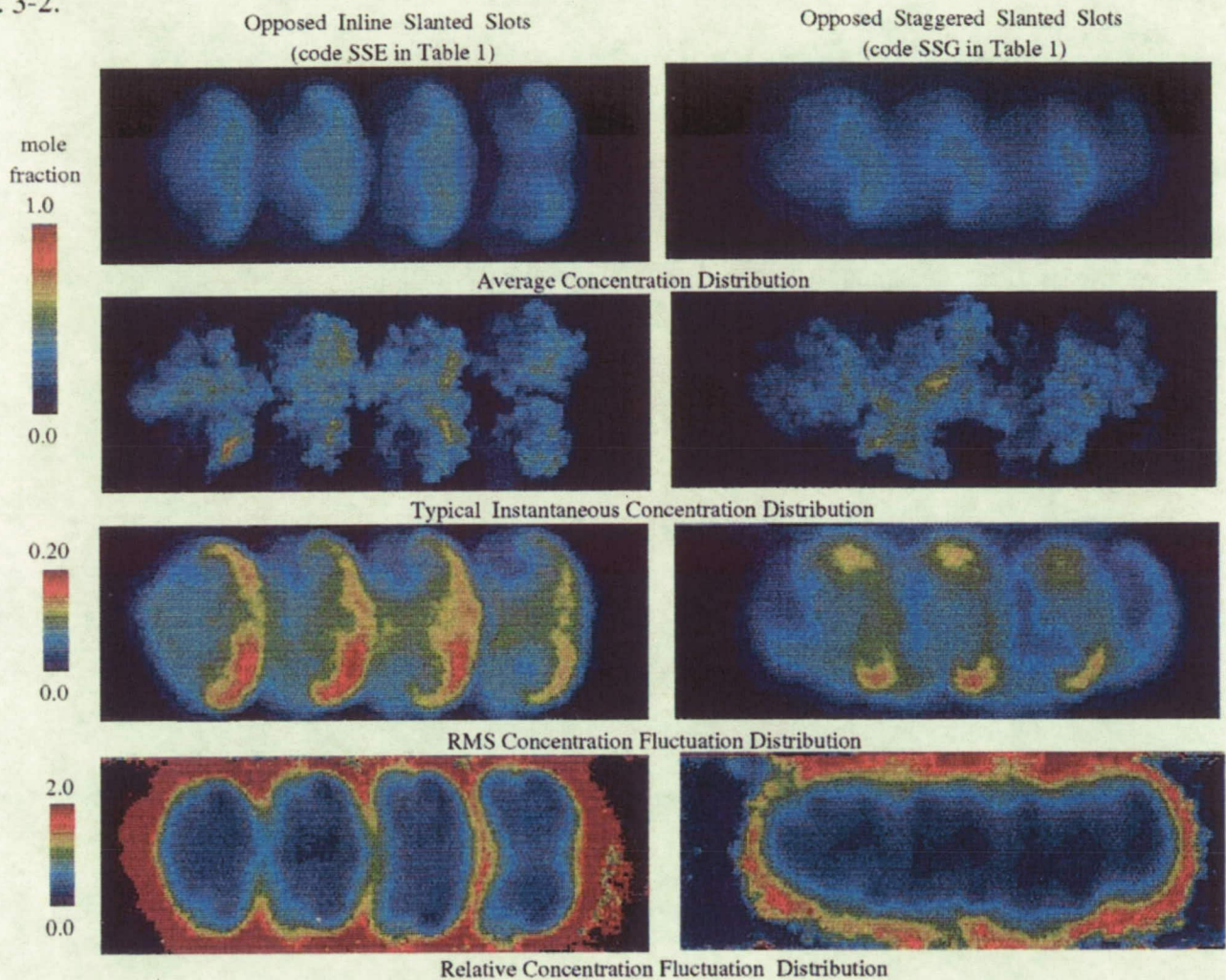


Figure 3-10: Concentration Distributions obtained from Time-resolved Measurements of the Flow through Opposed Inline 45° Slanted Slots. $J = 36$, $x/H = 0.33$

3.4.5 Concentration Probability Density Functions (pdf's)

Pdf's of time-resolved and local ensemble average, "spatial", distributions for opposed in-line jets (code SSE in Table 3-1) are compared in Fig. 3-11. Areas under the curves are unity. The instantaneous (Fig. 3-11a-c) and spatial (Fig. 3-11d) pdf's are similar. As would be expected, the range of fluctuations is greater in the time-resolved data; ensemble averaging truncates the distribution, consistent with a lower value of unmixedness, and the maximum measured mole fraction is reduced from about 0.60 to 0.45. The results indicate that much of the mixture inhomogeneity can be attributed to mean gradients and, the screening of configurations on the basis of ensemble averaged data should be justified in most cases.

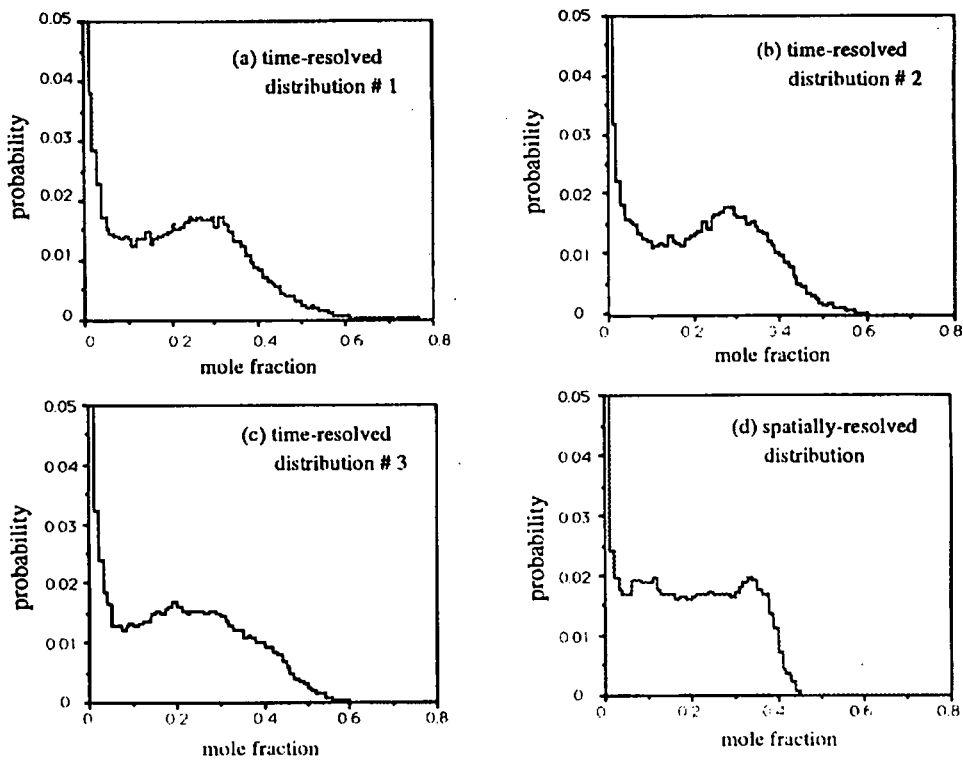


Figure 3-11: Probability Density Functions of Time-resolved (11a-c) and Spatially Averaged (11d) Concentration Distributions of Opposed Inline Slanted Slots , $J = 36$ and $x/H = 0.33$ (code SSE in Table 3-1)

Spatial pdf's for inline slanted slots (code SSE in Table 3-1) and round holes (code RHD in Table 3-1) at $J = 36$ are presented in Figs. 3-12 and 3-13, respectively. The mole fraction of the fully mixed fluid, C_{avg} , is also indicated. It is seen that, (1) the range of the fluctuations is greater with slot injection and, (2) the probability density representing pure mainstream fluid (i.e. mole fraction = 0) is more persistent in the slot configuration. In the round hole configuration, the peak at mole fraction = 0 is starting to decrease at $x/H = 1.06$. The pdfs are consistent with Fig. 3-6 which indicates that U_i is similar for both configurations.

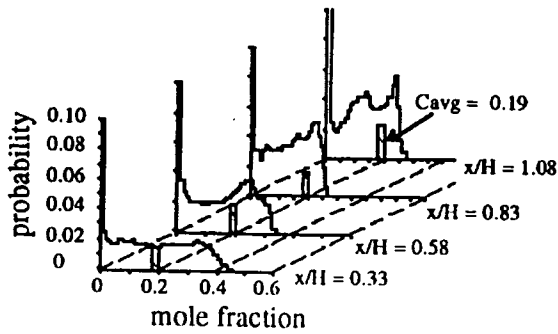


Figure 3-12: Probability Density Function for Opposed Inline Slanted Slots at $J = 36$ (code SSE in Table 3-1)

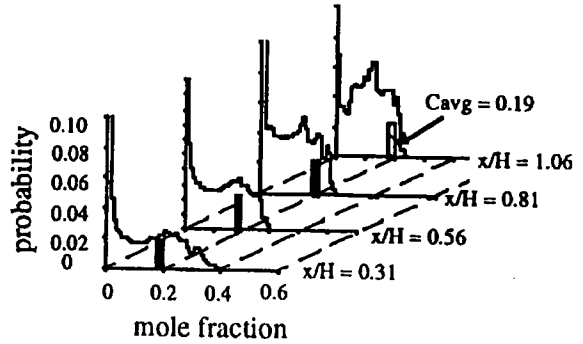


Figure 3-13: Probability Density Function for Opposed Inline Round Holes at $J = 36$ (code RHD in Table 3-1)

Pdf's of the opposed staggered slanted slot configuration (code SSG in Table 3-1) are shown in Fig. 3-14. U_i is considerably lower for this configuration (Fig 8), but despite lower unmixedness, the range of mole fractions is similar to the inline configuration. The initial mixing rate is more rapid than in the opposed inline slot configuration (code SSE in Table 3-1), as reflected in the narrower distribution away from the peak representing mainstream fluid at mole fraction = 0. The staggered slot pdf has a bimodal distribution with little qualitative change occurring with downstream position. Thus, most of the mixing occurs within the first inch of travel; the pdf's at $x/H = 0.83$ and 1.08 are nearly identical.

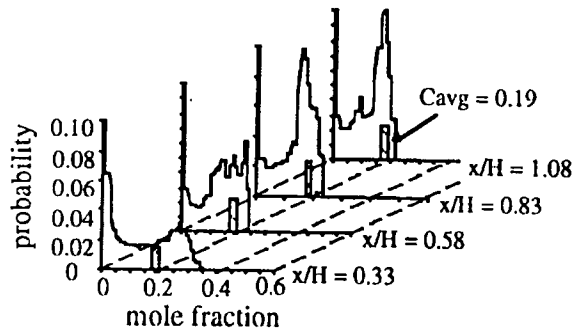


Figure 3-14: Probability Density Function for Opposed Staggered Slanted Slots at $J = 36$ (code SSG in Table 3-1)

3.4.6 Spatial Covariance

Information about turbulence scales is essential in modeling, as mentioned previously. Time-resolved, simultaneous, multi-point measurements allow calculation of spatial covariance from which turbulent integral length scale can be derived. By way of demonstration, covariance was calculated relative to a point located at the duct center plane for opposed inline slanted slots (code SSE in Table 3-1) at $x/H = 0.33$ and $J = 36$. Fluctuations were found to be correlated to a separation distance of about 0.3 inches. This suggests that an inhomogeneous reaction zone model would be appropriate, since chemical reactions would be expected to occur at smaller scale.

3.5 Conclusions

- Momentum-flux ratio and orifice geometry affect mixing performance significantly.
- Mixing rate increases continuously with momentum-flux ratio.
- The coupling between momentum-flux ratio and orifice spacing at the optimum mixing rate, given by Eq. 3-2, applies to slanted slots, however blockage is also an important parameter.
- Mixing rate is a function of slot orientation.
- At $S/H \geq 0.5$ the mixing rate for slanted slots and round holes is equivalent, although jet structure is different.
- Time-resolved measurements support conclusions based on U_s .
- The pdf's indicate little change in planar mixture distribution with distance.

3.6 References

- 3-1. Hatch, M.S., Sowa, W.A., Samuelson, G.S., and Holdeman, J.D., "Jet Mixing into Heated Cross Flow in a Cylindrical Duct: Influence of Geometry and Flow Variations on Mixing of Jets in a Heated Cross Flow," AIAA 92-0773, 30th Aerospace Sciences Meeting, Reno, Jan. 1992 (see also NASA TM 105390).
- 3-2. Holdeman, J.D., "Mixing of Multiple Jets with a Confined Subsonic Crossflow; Summary of NASA Supported Experiments and Modeling," AIAA Paper 91-2458, Sacramento, CA., June 1991 (see also NASA TM 104412).
- 3-3. Long, M.L., Chu, B.T., and Chang, R.K., "Instantaneous Two-Dimensional Gas Concentration Measurements by Light Scattering," AIAA Journal, Vol. 19, Sept. 1981, pp. 1151-1157.
- 3-4. Shaw, R.J., "Engine Technology Challenges for a 21st Century High Speed Civil Transport," AIAA 10th International Symposium on Air Breathing Engines, Sept. 1-6, 1991 (see also NASA TM 104361).
- 3-5. Smith, C.E., Talpallikar, M.V., and Holdeman, J.D., "A CFD Study of Jet Mixing in Reduced Flow Areas for Lower Combustor Emissions," AIAA Paper 91-2460, Sacramento, CA., June 1991 (see also NASA TM 104411).
- 3-6. Talpallikar, M.V., Smith, C.E., Lai, M.C., and Holdeman, J.D., "CFD Analysis of Jet Mixing in Low NO_x Flametube Combustors," ASME Paper 91-GT-217, Orlando, FL., June 1991 (see also NASA TM 104466).
- 3-7. Vranos, A. and Liscinsky, D.S., "Planar Imaging of Jet Mixing in Crossflow," AIAA Journal, 26, 11, Nov. 1988, pp. 1297-98.
- 3-8. Vranos, A., Liscinsky, D.S., True, B., and Holdeman, J.D., "Experimental Study of Cross-Stream Mixing in a Cylindrical Duct," AIAA Paper 91-2459, Sacramento, CA., June 24-27, 1991 (see also NASA TM 105180).

4. SUMMARY and CONCLUSIONS

The principle conclusions from the cylindrical and rectangular duct experiments are:

1. Mixing is primarily a function of momentum-flux ratio (J) and injector spacing.
2. Holdeman^{2-3 to 2-8} has shown for round holes in a rectangular duct that jet penetration and mixing is similar when orifice spacing and the square root of J are inversely proportional. This relationship also applied to a 45° slanted slot in a cylindrical duct for a configuration where the adjacent slots did not overlap. Blockage (the web between adjacent orifices) is also an important parameter for non-symmetrical orifices.
3. When equal area 45° slanted slot and round hole injectors were compared in a cylindrical duct in a configuration which had six equally spaced orifices, better mixing performance was observed for the slanted slots injectors at values $J > 20$. Round holes performed better than the slanted slots at lower values of J for the six injector configuration.
4. Unmixedness of slanted slots in a cylindrical duct is more sensitive to downstream distance than for round holes, which is in agreement with video tapes that show different jet/jet and jet/mainstream interactions for the two types of injectors.
5. For 45° slanted slots in a rectangular duct, mixing rate is a function of how the orifices are oriented on opposite walls of the duct.
6. Unmixedness values based on time-averaged and time-resolved measurements were found to be nearly equivalent.
7. Probability density functions of the concentration distributions indicate that most of the mixing occurs close to the point of injection.

REPORT DOCUMENTATION PAGE			Form Approved OMB No. 0704-0188	
Public reporting burden for this collection of information is estimated to average 1 hour per response, including the time for reviewing instructions, searching existing data sources, gathering and maintaining the data needed, and completing and reviewing the collection of information. Send comments regarding this burden estimate or any other aspect of this collection of information, including suggestions for reducing this burden, to Washington Headquarters Services, Directorate for Information Operations and Reports, 1215 Jefferson Davis Highway, Suite 1204, Arlington, VA 22202-4302, and to the Office of Management and Budget, Paperwork Reduction Project (0704-0188), Washington, DC 20503.				
1. AGENCY USE ONLY (Leave blank)	2. REPORT DATE April 1993	3. REPORT TYPE AND DATES COVERED Final Contractor Report		
4. TITLE AND SUBTITLE Experimental Study of Cross Flow Mixing in Cylindrical and Rectangular Ducts		5. FUNDING NUMBERS WU-537-02-20 NAS3-25952		
6. AUTHOR(S) D.S. Liscinsky, A. Vranos, and R.P. Lohmann		8. PERFORMING ORGANIZATION REPORT NUMBER E-7708		
7. PERFORMING ORGANIZATION NAME(S) AND ADDRESS(ES) United Technologies Research Center 411 Silver Lane East Hartford, Connecticut 06108		9. SPONSORING/MONITORING AGENCY NAMES(S) AND ADDRESS(ES) National Aeronautics and Space Administration Lewis Research Center Cleveland, Ohio 44135-3191		
9. SPONSORING/MONITORING AGENCY NAMES(S) AND ADDRESS(ES)		10. SPONSORING/MONITORING AGENCY REPORT NUMBER NASA CR-187141		
11. SUPPLEMENTARY NOTES Project Manager, J.D. Holdeman, Internal Fluid Mechanics Division, (216) 433-5846. D.S. Liscinsky, United Technologies Research Center, East Hartford, Connecticut 06108; A. Vranos, AB Research Associates, South Windsor, Connecticut 06074; and R.P. Lohmann, Pratt & Whitney Aircraft, East Hartford, Connecticut 06108.				
12a. DISTRIBUTION/AVAILABILITY STATEMENT Unclassified - Unlimited Subject Category 07		12b. DISTRIBUTION CODE		
13. ABSTRACT (Maximum 200 words) An experimental investigation of non-reacting cross flow jet injection and mixing in cylindrical and rectangular ducts has been conducted with application to a low emissions combustor. Quantitative measurement of injectant concentration distributions perpendicular to the duct axis were obtained by planar digital imaging of the Mie-scattered light from an aerosol seed mixed with the injectant. The flowfield unmixedness was evaluated using (1) a mixing parameter derived from the ratio of the jet concentration fluctuations to the fully mixed concentration, and (2) probability density functions of the concentration distributions. Mixing rate was measured for 45° slanted slot and round orifice injectors.				
14. SUBJECT TERMS Rectangular duct; Dilution; Jet mixing flow; Gas turbine; Combustion chamber; Can; Emissions			15. NUMBER OF PAGES 54	16. PRICE CODE A04
17. SECURITY CLASSIFICATION OF REPORT Unclassified	18. SECURITY CLASSIFICATION OF THIS PAGE Unclassified	19. SECURITY CLASSIFICATION OF ABSTRACT Unclassified	20. LIMITATION OF ABSTRACT	